

Contrastive Spectral Rectification: Test-Time Defense towards Zero-shot Adversarial Robustness of CLIP

Sen Nie^{1,2} Jie Zhang^{1,2} Zhuo Wang³ Shiguang Shan^{1,2} Xilin Chen^{1,2}

Abstract

Vision-language models (VLMs) such as CLIP have demonstrated remarkable zero-shot generalization, yet remain highly vulnerable to adversarial examples (AEs). While test-time defenses are promising, existing methods fail to provide sufficient robustness against strong attacks and are often hampered by high inference latency and task-specific applicability. To address these limitations, we start by investigating the intrinsic properties of AEs, which reveals that AEs exhibit severe feature inconsistency under progressive frequency attenuation. We further attribute this to the model’s inherent spectral bias. Leveraging this insight, we propose an efficient test-time defense named **Contrastive Spectral Rectification** (CSR). CSR optimizes a rectification perturbation to realign the input with the natural manifold under a spectral-guided contrastive objective, which is applied input-adaptively. Extensive experiments across 16 classification benchmarks demonstrate that CSR outperforms the SOTA by an average of **18.1%** against strong AutoAttack with modest inference overhead. Furthermore, CSR exhibits broad applicability across diverse visual tasks. Code is available at <https://github.com/Summu77/CSR>.

1 Introduction

Large-scale pre-trained Vision-Language Models (VLMs), notably CLIP (Radford et al., 2021), have revolutionized multimodal representation learning with their remarkable zero-shot generalization (Shen et al., 2022; Jing et al., 2024; Awais et al., 2025). Despite this success, CLIP models remain highly vulnerable to adversarial examples (Zhao et al., 2024; He et al., 2025). Imperceptible perturbations can easily deceive the model, undermining its reliability in safety-critical open-world applications (Chen et al., 2025a).

¹State Key Laboratory of AI Safety, Institute of Computing Technology, Chinese Academy of Sciences, China, Beijing

²University of Chinese Academy of Sciences, China, Beijing

³University of Science and Technology of China, China, Hefei. Correspondence to: Jie Zhang <zhangjie@ict.ac.cn>.

Preprint. January 28, 2026.

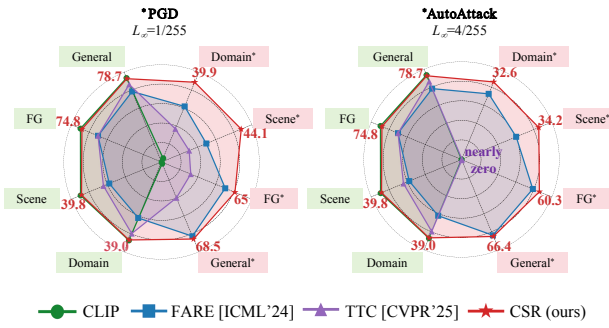


Figure 1. Zero-shot adversarial robustness comparison. We evaluate our **CSR** against **CLIP**, **FARE** (adversarial fine-tuning), and **TTC** (test-time defense) on 16 datasets grouped into General, Fine-Grained (FG), Scene, and Domain. The radar charts show Top-1 accuracy on benign and adversarial samples under standard PGD ($\ell_\infty = 1/255$) and the stronger AutoAttack ($\ell_\infty = 4/255$).

To mitigate this vulnerability, Adversarial Fine-tuning (AFT) (Mao et al., 2023; Wang et al., 2024b) is a straightforward defense strategy by fine-tuning the model on adversarial examples. However, AFT incurs prohibitive computational costs for large-scale models and often severely degrades the model’s performance on benign samples, as illustrated by FARE (Schlarmann et al., 2024) in Figure 1. Consequently, test-time defense has emerged as a promising alternative (Zhang et al., 2025b; Tong et al., 2025), aiming to purify inputs during inference without retraining. However, current methods often suffer from high inference latency (Zhu et al., 2025) and exhibit sub-optimal performance especially under strong attacks. For instance, as shown in Figure 1, TTC (Xing et al., 2025) collapses under stronger AutoAttack (Croce & Hein, 2020), yielding marginal robustness gains. Moreover, many defenses are inherently designed for specific scenarios (Li et al., 2024b; Sheng et al., 2025; Wang et al., 2025a), limiting their applicability to broader visual tasks such as Segmentation, Image Captioning, and Visual Question Answering (VQA). Therefore, developing an effective, efficient, and universal test-time defense for CLIP remains a critical challenge.

To this end, we start by investigating the intrinsic properties of adversarial examples (AEs). Intuitively, subtle adversarial perturbations should be fragile; however, prior efforts applying random noise to adversarial examples (Xing et al., 2025) failed to substantiate this property. We thus turn to the fre-

quency domain, analyzing feature consistency via progressive frequency attenuation. As shown in Figure 3, benign features degrade smoothly with the progressive removal of mid-to-high frequencies, whereas adversarial features suffer a sharp decay, revealing a severe fragility across diverse attacks. We trace this phenomenon to a two-fold vulnerability intrinsic to CLIP: its spectral bias toward mid-to-high frequencies and its hypersensitivity to perturbations within these bands. Consequently, adversarial attacks inevitably exploit these high-impact spectral regions, rendering AEs inherently fragile to such spectral filtering.

Motivated by this insight, we propose **Contrastive Spectral Rectification** (CSR), an efficient test-time defense method. Unlike the naive adoption of low-pass filtered features, CSR introduces an active mechanism that optimizes a learnable rectification perturbation superimposed onto the input image. Specifically, we formulate a contrastive objective where the low-pass filtered feature serves as a positive anchor and the original feature as a negative anchor. This objective drives the rectification perturbation to repel the image from the adversarial subspace and realign it with the natural manifold, as depicted in Figure 2. To ensure efficiency and maintain performance on benign examples, we incorporate an input-adaptive gating mechanism: by measuring feature consistency before and after spectral filtering, CSR triggers the rectification process only for samples exhibiting adversarial instability. Consequently, CSR leverages the intrinsic spectral properties of CLIP to efficiently detect and rectify adversarial examples at inference without retraining.

Through extensive experiments across 16 zero-shot classification benchmarks, we demonstrate that CSR consistently outperforms state-of-the-art defenses. Specifically, it achieves an average improvement of 6.9% against standard PGD and a substantial **18.1%** gain against the stronger AutoAttack, while maintaining accuracy on benign samples. Notably, CSR delivers this superior robustness with modest inference overhead, offering a highly efficient test-time solution. Furthermore, CSR generalizes effectively to diverse visual tasks, including Semantic Segmentation, Image Captioning, and VQA, highlighting its broad applicability.

Our contributions are as follows:

- We uncover a spectral fragility in adversarial examples and trace this vulnerability to CLIP’s spectral bias and sensitivity to mid-to-high frequency components.
- We introduce CSR, a test-time defense that utilizes a spectral-guided contrastive rectification and an input-adaptive gating mechanism to efficiently detect and purify adversarial examples during inference.
- We validate CSR across 16 benchmarks, where it delivers state-of-the-art robustness (e.g., +18.1% against AutoAttack) with high inference efficiency. Beyond classification, CSR also proves effective in diverse tasks.

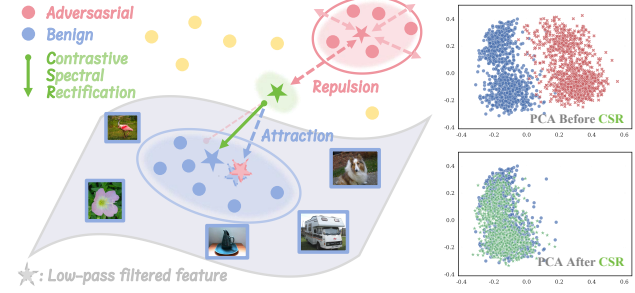


Figure 2. Mechanism of Contrastive Spectral Rectification (CSR). Leveraging a spectral contrastive strategy, CSR exerts **repulsion** from the original adversarial feature (solid red star) within the *adversarial subspace*, while inducing **attraction** toward the low-pass filtered feature (dashed red star)—an approximation on the *benign manifold*. This synergy steers the optimization toward the ground-truth feature (solid blue star), effectively rectifying the feature space as corroborated by the PCA visualization (right) on 300 images.

2 Preliminaries and Related Work

Large pre-trained Vision-Language Models (VLMs), notably CLIP (Radford et al., 2021), learn aligned multimodal representations via contrastive learning, enabling remarkable zero-shot generalization across various tasks.

Zero-shot Classification with CLIP. Representatively, CLIP can leverage its cross-modal alignment to categorize images into open-vocabulary classes without task-specific fine-tuning. Formally, let $f(\cdot)$ and $g(\cdot)$ denote the image and text encoders, respectively. Given an input image \mathbf{x} and a set of K candidate classes, we construct textual prompts $\{\mathbf{t}_i\}_{i=1}^K$ using a template (e.g., “a photo of a {class}”). Let $\mathbf{z}_v = f(\mathbf{x})/\|f(\mathbf{x})\|_2$ and $\mathbf{z}_{t,i} = g(\mathbf{t}_i)/\|g(\mathbf{t}_i)\|_2$ be the L_2 -normalized visual and textual embeddings. The zero-shot prediction probability for the i -th class is computed via the softmax-normalized cosine similarities:

$$p(y_i|\mathbf{x}) = \frac{\exp(\tau \cdot \mathbf{z}_v^\top \mathbf{z}_{t,i})}{\sum_{j=1}^K \exp(\tau \cdot \mathbf{z}_v^\top \mathbf{z}_{t,j})}, \quad (1)$$

where τ is a temperature parameter for scaling, and the predicted label is given by $\hat{y} = \arg \max_i p(y_i|\mathbf{x})$.

Adversarial Attacks on CLIP. Despite its impressive generalization, CLIP remains susceptible to adversarial perturbations. Formally, attackers seek an imperceptible perturbation δ within an ℓ_p -norm budget ϵ to maximize the loss \mathcal{L} , typically the cross-entropy loss for classification:

$$\max_{\delta} \mathcal{L}(f(\mathbf{x} + \delta), g(\mathbf{t}_y)) \quad \text{s.t.} \quad \|\delta\|_p \leq \epsilon. \quad (2)$$

Standard methods, such as PGD (Madry et al., 2017) and the stronger AutoAttack (Croce & Hein, 2020), employ iterative gradient ascent to optimize this perturbation by leveraging the loss gradient ($\nabla_{\mathbf{x}} \mathcal{L}$). A more extensive review of adversarial attacks on (L)VLMs is deferred to Appendix A.

To mitigate these threats, various defenses have emerged, generally falling into adversarial training and test-time defense.

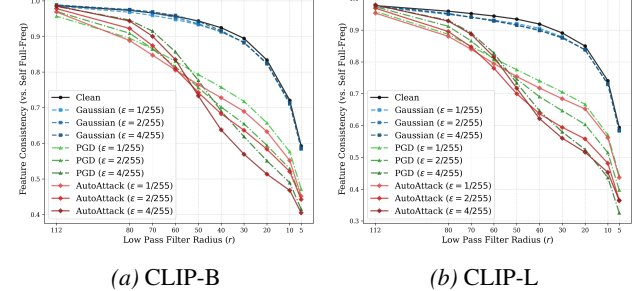
Adversarial Training for VLMs. Early strategies, termed Adversarial Fine-Tuning, enhance robustness by fine-tuning models on adversarial examples. Approaches like TeCoA (Mao et al., 2023) and PMG-AFT (Wang et al., 2024b) introduce auxiliary objectives to mitigate catastrophic forgetting (Wang et al., 2024c; Dong et al., 2025b; Sui et al., 2025; Dong et al., 2025c), while FARE (Schlarmann et al., 2024) and Sim-CLIP+ (Hossain & Imteaj, 2024) employ unsupervised learning to improve robustness transferability. However, the prohibitive cost of full fine-tuning has shifted focus toward Adversarial Prompt Tuning, leveraging parameter-efficient techniques (Ding et al., 2023; Han et al., 2024). By optimizing learnable prompts while keeping the backbone frozen, methods such as VPT (Mao et al., 2023), APT (Li et al., 2024a), FedAPT (Zhai et al., 2025), and AdvPT (Zhang et al., 2024a) effectively align text embeddings with adversarial visual features. Subsequent works (e.g., FAP (Zhou et al., 2024b), CoAPT (Wang et al., 2025c)) further advance this paradigm by incorporating few-shot regimes and structural priors. Despite these improvements, these methods frequently entail high training costs and risk compromising benign performance or overfitting.

Test-Time Defense for VLMs. Drawing inspiration from Test-Time Adaptation (Shu et al., 2022; Abdul Samad et al., 2023; Dong et al., 2025a; Chen et al., 2025c; Zhou et al., 2025; Hu et al., 2025), recent research focuses on enhancing CLIP’s robustness at inference without retraining. One direction focuses on textual alignment (Zhou et al., 2024a; Hussein et al., 2024): TAPT (Wang et al., 2025a), RTPT (Sheng et al., 2025), and D-TPT (Han & Hwang, 2025) employ entropy-based prompt tuning, while COLA (Zhu et al., 2025) formulates the alignment as an optimal transport problem. Parallel efforts target visual purification (Deng et al., 2025; Su & Balogh, 2025): CLIPure (Zhang et al., 2025b) leverages diffusion priors, while TTE (Pérez et al., 2021), DDA (Reyes-Amezcua et al., 2024), and AOM (Tong et al., 2025) utilize transformation ensembles. Closest to our work is TTC (Xing et al., 2025), which updates inputs to counteract perturbations. However, its only focus on escaping the adversarial subspace without benign guidance distorts natural semantics, thereby limiting its efficacy. Overall, existing methods remain constrained by their vulnerability to strong attacks, high inference latency, and limited task-specific applicability, motivating our proposal of an effective, efficient, and universal test-time defense method.

3 Insight

3.1 Observation: Disparity in Feature Consistency

To motivate our test-time defense, we first investigate the intrinsic properties of adversarial examples (AEs). Specifically, we analyze the spectral consistency of CLIP by examining the stability of feature representations under low-pass filtering. Using 1,000 images sampled from ImageNet, we



(a) CLIP-B

(b) CLIP-L

Figure 3. Spectral Consistency Disparity. Cosine similarity between original and low-pass filtered embeddings across decaying bandwidth radii r . While benign examples maintain high semantic fidelity, adversarial examples exhibit rapid feature collapse. See Appendix C for consistent trends across additional datasets.

apply filters with decaying bandwidth radii r to three categories: clean images, Gaussian-corrupted counterparts, and AEs generated via PGD (Madry et al., 2017) and AutoAttack (Croce & Hein, 2020). We quantify feature resilience using the cosine similarity between the filtered and original embeddings. As shown in Figure 3, a divergence emerges:

(i) Stability of Benign Examples (BEs): Benign Examples, encompassing both clean inputs and Gaussian-noised counterparts, exhibit high feature stability, maintaining semantic fidelity even under aggressive frequency truncation. Notably, samples corrupted with Gaussian noise show negligible feature divergence from the clean baseline, even at relatively high noise budgets of $\ell_\infty = 4/255$.

(ii) Fragility of Adversarial Examples (AEs): In contrast, AEs suffer from abrupt degradation in feature consistency as mid-to-high frequency components are removed. This vulnerability is pronounced even at minimal noise budgets (e.g., $\ell_\infty = 1/255$) and persists across diverse attack variants. This indicates that adversarial deceptive signals are critically reliant on mid-to-high frequency components.

Discussion. We attribute the resilience of BEs to the robust semantic priors instilled by large-scale pre-training. This fosters a strong shape bias (Naseer et al., 2021), guiding the model to prioritize structural representations that reside firmly on the low-dimensional manifold of natural images. However, the divergent behavior of AEs prompts a fundamental question: *Why do adversarial perturbations inherently gravitate toward the mid-to-high frequency spectrum, and in what ways does this spectral bias bolster their deceptive efficacy?* We explore the underlying mechanisms of this frequency preference in the following subsection.

3.2 Analysis: Spectral Bias and Sensitivity of CLIP

Since AEs are crafted to maximize model error under constrained budgets, their consistent gravitation toward mid-to-high frequency components suggests a spectral vulnerability within CLIP. To deconstruct this, we examine the spectral

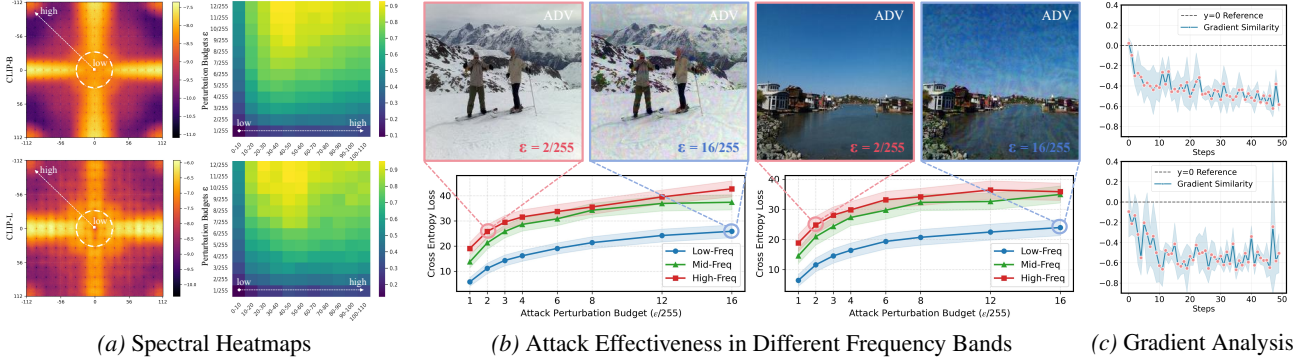


Figure 4. Analysis. (a) The gradient magnitude (left) and representational shift (right) are concentrated in mid-to-high frequency components, indicating that the model is most vulnerable to perturbations in these bands. (b) Attacks constrained to low frequencies are inefficient. (c) The adversarial gradient exhibits consistent negative cosine similarity with the low-frequency constraint gradient.

density of loss gradients and quantify the representational shift induced by band-specific perturbations.

(i) Intrinsic Spectral Bias: We formally characterize the sensitivity of the model’s objective function with respect to the input’s frequency components. Let $\mathcal{F}(\mathbf{x}) \in \mathbb{C}^{H \times W}$ denote the 2D Discrete Fourier Transform of input \mathbf{x} . We define the **Spectral Gradient Magnitude** (SGM), $\mathcal{S} \in \mathbb{R}^{H \times W}$, as the expected magnitude of the gradient of the loss \mathcal{L} with respect to the spectral amplitude:

$$\mathcal{S}(u, v) = \mathbb{E}_{\mathbf{x} \sim \mathcal{D}} \left[\left\| \nabla_{|\mathcal{F}(\mathbf{x})_{u, v}|} \mathcal{L}(f(\mathbf{x}), g(\mathbf{t}_y)) \right\|_2 \right], \quad (3)$$

where (u, v) represents the spatial frequency coordinates. As visualized in Figure 4a (Left), the heatmap of \mathcal{S} reveals a distinct vulnerability: CLIP exhibits significant gradient responses $\nabla \mathcal{L}$ extending well into the mid-to-high frequency periphery (the area outside the white dashed circle). This distribution uncovers a spectral bias: unlike human perception, which is robustly anchored in low-frequency semantics (e.g., shape), CLIP places disproportionate predictive weight on mid-to-high frequency patterns. These components, identified as non-robust features (Ilyas et al., 2019), yield steep gradients and serve as an accessible “discriminative shortcut” for attackers to efficiently manipulate model predictions.

(ii) Spectral Feature Hypersensitivity: We quantify the sensitivity of CLIP’s feature representations to band-specific spectral perturbations. We measure the worst-case feature space displacement induced by attacks restricted to specific frequency bands. Let \mathbf{M}_k be a binary mask isolating the k -th frequency band. We solve for the optimal perturbation δ_k that maximizes the feature drift Δ_Φ with PGD:

$$\begin{aligned} \max_{\delta_k} \Delta_\Phi &= 1 - \frac{f(\mathbf{x})^\top f(\mathbf{x} + \mathcal{F}^{-1}(\mathbf{M}_k \odot \mathcal{F}(\delta_k)))}{\|f(\mathbf{x})\|_2 \|f(\mathbf{x} + \mathcal{F}^{-1}(\mathbf{M}_k \odot \mathcal{F}(\delta_k)))\|_2}, \\ \text{s.t. } \|\delta_k\|_\infty &\leq \epsilon. \end{aligned} \quad (4)$$

The results in Figure 4a (Right) reveal a sensitivity imbalance. While perturbations restricted to low-frequency bands (e.g., 0-30) induce small feature shifts Δ_Φ , especially

under low noise budgets ($\ell_\infty < 4/255$), those targeting mid-to-high frequency bands trigger large representational deviations. This indicates that the model’s representation is hypersensitive to mid-to-high frequency components. Consequently, these bands constitute a structural vulnerability, allowing minimal noise to efficiently displace the image embedding from its natural semantic manifold.

Finally, we investigate the effectiveness of attacks across different frequency bands. Our analysis reveals an efficiency-imperceptibility trade-off, as shown in Figure 4b. Specifically, confining perturbations to the low-frequency band results in inefficiency, necessitating prohibitive budgets (e.g., $\ell_\infty = 16/255$) to match the damage of high-frequency attacks (e.g., $\ell_\infty = 2/255$). This magnitude amplification introduces conspicuous wavy artifacts, thereby violating the imperceptibility premise. We attribute this to an inherent gradient incompatibility. As evidenced in Figure 4c (and theoretical analysis in Appendix B), the gradient for adversarial aggressiveness exhibits consistent negative cosine similarity with that of low-frequency confinement. Driven by this optimization landscape, **attacks naturally gravitate toward the mid-to-high frequency bands to maximize efficiency**.

4 Method

Building on the spectral insights derived in Section 3, we propose **Contrastive Spectral Rectification** (CSR), a test-time defense framework designed to robustify CLIP against adversarial perturbations without retraining. The overall procedure is summarized in Algorithm 1.

4.1 Adversarial Detection via Spectral Consistency

The first step of CSR involves the input-adaptive gating mechanism. We employ a Gaussian low-pass filter $G(\cdot)$ with a filter radius r to attenuate mid-to-high frequency components, yielding a smoothed counterpart $\mathbf{x}_{low} = G(\mathbf{x})$. As established in Section 3, benign samples exhibit strong feature consistency between their full-spectrum and low-frequency representations. Conversely, for adversarial examples, the removal of mid-to-high frequency components leads to a

Algorithm 1 Contrastive Spectral Rectification (CSR)

Require: Input image \mathbf{x} ; CLIP image encoder $f(\cdot)$; LPF operator $G_r(\cdot)$ with radius r ; detection threshold τ ; perturbation budget ϵ ; rectification steps N ; step size α .

Ensure: Rectified reliable image \mathbf{x}^*

```

1:  $\mathbf{z} \leftarrow f(\mathbf{x}), \mathbf{z}_{low} \leftarrow f(G_r(\mathbf{x}))$ 
2:  $s \leftarrow \cos(\mathbf{z}, \mathbf{z}_{low}) \triangleright (i) \text{ Adversarial Examples Detection}$ 
3: if  $s \geq \tau$  then
4:   return  $\mathbf{x}$             $\triangleright \text{Consistent} \rightarrow \text{Benign Image}$ 
5: else
6:    $\delta \leftarrow \mathbf{0}, \mathbf{x}' \leftarrow \mathbf{x} + \delta, \mathbf{x}^* \leftarrow \mathbf{x}, \mathcal{L}_{best} \leftarrow -\infty$ 
7:   for  $t = 1$  to  $N$  do
8:      $\triangleright (ii) \text{ Few-step Contrastive Spectral Rectification}$ 
9:      $\mathbf{z}' \leftarrow f(\mathbf{x}')$ 
10:     $\mathcal{L}_{rec} \leftarrow \cos(\mathbf{z}', \mathbf{z}_{tgt}) - \cos(\mathbf{z}', \mathbf{z}_{adv})$ 
11:    if  $\mathcal{L}_{rec} > \mathcal{L}_{best}$  then
12:       $\mathcal{L}_{best} \leftarrow \mathcal{L}, \mathbf{x}^* \leftarrow \mathbf{x}' \triangleright (iii) \text{ Greedy Selection}$ 
13:    end if
14:     $\mathbf{x}' \leftarrow \mathbf{x}' + \text{clip}(\delta + \alpha \cdot \text{sign}(\nabla_{\mathbf{x}'} \mathcal{L}), -\epsilon, \epsilon)$ 
15:   end for
16: end if
17: return  $\mathbf{x}^*$             $\triangleright \text{Return Rectified Reliable Image}$ 

```

significant feature collapse. We quantify this divergence using the Cosine Similarity between the embeddings:

$$\mathcal{C}(\mathbf{x}) = \frac{f(\mathbf{x})^\top f(\mathbf{x}_{low})}{\|f(\mathbf{x})\|_2 \|f(\mathbf{x}_{low})\|_2}. \quad (5)$$

A high $\mathcal{C}(\mathbf{x})$ indicates that the semantic content is robustly anchored in the low-frequency band, characteristic of BEs. Conversely, a low score reveals a reliance on fragile mid-to-high frequencies—a signature of AEs. We classify an input as adversarial if $\mathcal{C}(\mathbf{x}) < \tau$, where τ is a detection threshold to balance detection sensitivity and the false positive rate. Detection ROC curves are provided in Appendix D.

4.2 Contrastive Spectral Rectification

While filtering is effective for detection, naive application of low-pass filters risks over-smoothing, eroding fine-grained details essential for zero-shot recognition. To overcome this, we propose Contrastive Spectral Rectification. Instead of the passive suppression of mid-to-high frequency components, CSR formulates an active test-time optimization that reconstructs a reliable input \mathbf{x}^* from the adversarial query.

We freeze the model parameters and optimize a rectification perturbation δ to get the rectified sample $\mathbf{x}' = \mathbf{x} + \delta$. The objective function, \mathcal{L}_{rec} , is designed as follows:

$$\mathcal{L}_{rec}(\delta) = \underbrace{\text{sim}(f(\mathbf{x} + \delta), f(\mathbf{x}_{low}))}_{\text{Attraction Term}} - \lambda \cdot \underbrace{\text{sim}(f(\mathbf{x} + \delta), f(\mathbf{x}))}_{\text{Repulsion Term}}, \quad (6)$$

where $\text{sim}(\cdot, \cdot)$ denotes cosine similarity and λ is a hyperparameter to balance the two terms.

- **Attraction Term:** We utilize the low-frequency anchor $f(\mathbf{x}_{low})$ as a benign semantic guide to pull the optimization trajectory back towards the robust natural manifold.

- **Repulsion Term:** To prevent stagnation in the adversarial state, this term pushes the sample away from the initial malicious adversarial embedding $f(\mathbf{x})$.

We solve Eq. (6) using Projected Gradient Descent (PGD) for a limited number of steps N . However, simply taking the final step’s output is suboptimal, as the optimization trajectory on the non-convex manifold may oscillate. To ensure the reliability of the rectified sample, we adopt a **Greedy Selection** strategy. Specifically, during the optimization process, we monitor \mathcal{L}_{rec} at each step t and maintain the candidate \mathbf{x}^* that achieves the maximum objective value:

$$\mathbf{x}^* = \mathbf{x} + \arg \max_{\delta_t \in \{\delta_1, \dots, \delta_N\}} \mathcal{L}_{rec}(\delta_t). \quad (7)$$

This strategy ensures that the returned sample corresponds to the state of maximal spectral consistency and adversarial divergence, providing a stable input for the final inference.

5 Experiments

5.1 Setup

Datasets and Models. Following previous work, we employ a comprehensive benchmark suite of 16 datasets. Specifically, we evaluate on general object recognition (ImageNet (Deng et al., 2009), CIFAR-10/100 (Krizhevsky et al., 2009), STL10 (Coates et al., 2011), Caltech-101/256 (Fei-Fei et al., 2004; Griffin et al., 2007)), fine-grained classification (OxfordPets (Parkhi et al., 2012), Flowers102 (Nilsback & Zisserman, 2008), Food101 (Bossard et al., 2014), StanfordCars (Krause et al., 2013)), scene recognition (SUN397 (Xiao et al., 2010), Country211 (Radford et al., 2021)), and domain-specific applications (FGVCAircraft (Maji et al., 2013), EuroSAT (Helber et al., 2019), DTD (Cimpoi et al., 2014), PCAM (Veeling et al., 2018)). Furthermore, we conduct experiments on various tasks using the VOC2010 (Everingham et al., 2010) and MS-COCO (Lin et al., 2014) datasets. We adopt CLIP ViT-B/16 as default and also conduct experiments on ViT-B/32, ViT-L/14, and ViT-L/14@336px (LLaVA visual encoder).

Implementation Details. Unless otherwise specified, we set the perturbation budget to 1/255 and the number of attack steps to 10 for PGD (Madry et al., 2017) and 50 for AutoAttack (Croce & Hein, 2020). For our CSR, we set the Gaussian filter radius $r = 40$, the detection threshold $\tau = 0.85$, the noise budget is set to 4/255, with a step size of 2/255, and the number of iterations to 3. We provide additional experimental details in Appendix E.1.

Comparison Methods. We evaluate our proposed method against existing state-of-the-art defenses. The comparison set comprises Test-Time Defense—specifically TTE (Pérez

Table 1. Top-1 zero-shot classification accuracy (%) under 10-step PGD attacks ($\ell_\infty = 1/255$). “Clean” and “Rob.” denote accuracies on benign and adversarial samples, respectively. The final two columns report the performance of our CSR compared to the original CLIP.

Dataset		Original Adversarial Fine-tuning						Test-Time Defense								Δ							
		CLIP		TeCoA		FARE		R-TPT		LPF		HD		Anti-Adv		TTE		TTC		CSR (Ours)			
Type	Name	Clean	Rob.	Clean	Rob.	Clean	Rob.	Clean	Rob.	Clean	Rob.	Clean	Rob.	Clean	Rob.	Clean	Rob.	Clean	Rob.	Clean	Rob.		
General	ImageNet	63.9	0.0	56.3	53.6	48.0	46.7	66.7	51.0	58.1	30.5	59.7	4.1	61.5	23.9	66.2	23.2	40.9	27.8	62.5	58.9	-1.4	+58.9
	CIFAR10	88.1	0.5	63.7	63.8	61.4	61.2	81.6	69.2	89.0	40.4	84.1	11.8	82.8	63.5	85.5	29.8	90.0	28.2	87.2	75.0	-0.9	+74.5
	CIFAR100	59.6	0.1	37.9	37.8	36.2	36.2	51.8	36.4	63.4	19.6	57.6	7.9	51.5	34.9	60.4	14.2	63.1	11.1	59.4	45.3	-0.2	+45.2
	STL10	97.5	4.8	90.7	90.6	92.0	92.0	96.8	92.7	96.9	77.6	96.8	34.0	97.2	83.1	97.6	75.6	96.4	51.1	97.2	87.5	-0.3	+82.7
	Caltech101	83.5	1.3	77.1	76.3	83.7	82.0	86.1	80.9	81.3	65.6	82.6	28.4	82.3	58.2	87.2	61.2	75.8	31.3	83.2	75.3	-0.3	+74.0
	Caltech256	83.5	1.5	72.0	69.5	78.4	77.6	88.0	80.5	82.8	66.5	80.4	20.9	81.6	55.8	87.3	59.4	73.4	41.8	82.9	76.6	-0.6	+75.1
Fine-Gained	OxfordPets	88.9	0.0	71.3	69.3	79.3	74.3	85.8	68.3	79.4	41.7	84.2	4.0	86.5	36.7	84.8	12.5	78.8	27.0	88.9	65.9	+0.0	+65.9
	Flowers102	66.0	0.0	21.3	21.5	41.7	38.7	65.8	48.8	59.8	33.1	63.3	3.5	63.5	25.3	65.3	5.5	55.8	23.3	65.8	53.5	-0.2	+53.5
	Food101	84.8	0.0	30.6	29.2	47.0	44.5	86.6	68.9	79.6	38.6	86.0	1.1	83.9	29.3	85.3	24.8	57.5	33.2	81.9	80.7	-2.9	+80.7
	StanfordCars	65.2	0.0	32.9	23.6	70.7	67.9	68.6	45.4	54.0	16.9	57.8	1.4	62.5	13.7	59.0	14.4	46.6	20.2	62.7	60.9	-2.5	+60.9
Scene	SUN397	63.6	0.2	39.9	37.2	47.6	45.7	64.1	53.1	59.2	31.3	59.7	4.0	62.5	22.7	65.4	20.2	47.5	26.2	63.0	66.3	-0.6	+66.1
	Country211	17.0	0.0	3.0	2.7	4.4	3.9	19.2	8.9	14.7	2.5	15.1	0.0	15.2	1.9	15.8	0.3	10.2	4.4	16.6	22.9	-0.4	+22.9
Domain	FGVCAircraft	23.1	0.0	5.2	7.9	12.2	12.6	23.8	16.7	17.8	7.2	18.8	1.3	20.4	6.0	23.3	4.9	13.8	10.6	22.7	31.2	-0.4	+31.2
	EuroSAT	42.9	0.0	16.5	16.4	12.6	12.6	29.6	22.3	41.6	4.9	41.7	8.5	38.7	25.5	42.3	8.3	45.6	10.2	42.9	40.4	+0.0	+40.4
	DTD	42.3	0.1	29.9	29.3	35.3	34.3	44.2	36.2	40.5	26.7	40.4	8.5	40.6	22.1	41.9	20.6	35.7	22.1	41.9	39.1	-0.4	+39.1
	PCAM	48.4	7.4	48.8	48.8	51.7	51.7	54.6	39.2	48.6	48.4	36.1	48.5	48.2	44.3	4.3	48.2	23.3	48.5	50.3	+0.1	+42.9	
All	Avg.	63.6	1.0	43.6	42.3	50.1	48.9	63.3	51.2	56.7	34.5	61.0	11.0	61.2	34.4	63.2	23.7	55.0	24.5	62.9	58.1	-0.7	+57.1

Table 2. Top-1 zero-shot classification accuracy (%) under stronger adversarial attacks (50-step PGD and AutoAttack, $\ell_\infty = 4/255$).

Method	General			Fine-Grained			Scene			Domain		
	Clean	PGD	AutoAttack	Clean	PGD	AutoAttack	Clean	PGD	AutoAttack	Clean	PGD	AutoAttack
CLIP	79.4	0.0	0.0	76.2	0.0	0.0	40.3	0.0	0.0	39.2	0.0	0.0
TeCoA	66.3	65.1	65.0	39.0	35.8	35.7	21.5	20.0	19.7	25.1	25.5	25.5
FARE	66.6	65.8	65.4	59.7	55.7	55.2	26.0	24.2	24.2	28.0	27.8	27.6
R-TPT	78.5	36.2	28.4	76.7	46.4	42.8	41.7	26.7	26.4	38.1	27.5	23.2
TTE	80.7	13.4	11.5	73.6	1.7	0.4	40.6	1.2	1.4	38.0	13.4	11.5
LPF	78.6	37.4	30.8	68.2	11.3	8.2	37.0	8.0	6.9	37.1	18.6	16.7
HD	76.9	0.5	0.1	72.8	0.0	0.0	37.4	0.0	0.0	37.3	0.1	0.0
Anti-Adv	76.2	22.6	2.7	74.1	1.7	0.0	38.9	1.1	0.2	37.1	9.8	1.7
TTC	73.3	14.7	0.6	59.7	2.0	0.0	28.9	1.2	0.0	35.8	9.3	0.3
CSR	78.7 ^{↓0.7}	78.0 ^{↑78.0}	66.4 ^{↑66.4}	74.8 ^{↓1.4}	75.4 ^{↑75.4}	60.3 ^{↑60.3}	39.8 ^{↓0.5}	43.8 ^{↑43.8}	34.2 ^{↑34.2}	39.0 ^{↓0.2}	43.2 ^{↑43.2}	32.6 ^{↑32.6}

Table 3. Running time per image (ms) (↓) on single RTX 4090.

Time	CLIP	R-TPT	HD	Anti-Adv	TTE	TTC	CSR(ours)
T_{Clean}	3.37	176.45	184.43	32.39	5.43	33.24	4.16
$T_{Rob.}$	3.37	176.20	189.34	32.44	5.41	35.13	26.18
$T_{Avg.}$	3.37	176.33	189.34	32.42	5.42	35.19	15.17

Table 4. Evaluation on different attack objectives, $\ell_\infty = 4/255$.

Method	Clean	Cross-Modal		Targeted		Label-free		
		PGD	AA	PGD	DLR	AA	PGD	AA
CLIP	63.9	0.0	0.0	0.0	0.0	0.1	0.0	0.0
FARE	48.0	46.2	45.9	46.7	46.3	46.3	46.6	46.0
TTC	40.9	2.7	0.3	25.4	6.8	6.2	10.2	1.6
CSR	62.5	60.3	60.1	46.9	46.4	45.0	49.7	47.6

et al., 2021), HD (Wu et al., 2021), Anti-Adv (Alfarra et al., 2022), LPF (Ziyadinov & Tereshonok, 2023), TTC (Xing et al., 2025), and R-TPT (Sheng et al., 2025). Adversarial fine-tuning baselines, such as TeCoA (Mao et al., 2023) and FARE (Schlarmann et al., 2024) (fine-tuned on ImageNet), are also included. Baselines are implemented using their original hyperparameter settings to ensure a fair comparison.

5.2 Main Results

Results on 16 Datasets. Table 1 presents a comprehensive evaluation of zero-shot classification robustness across 16 datasets. Adversarial fine-tuning (e.g., TeCoA, FARE) suffers from severe benign performance degradation (↓ 20% and ↓ 13%, respectively) due to catastrophic forgetting. Among test-time methods, R-TPT achieves competitive robustness but incurs high inference latency—approximately 12× that of CSR (see Table 3). Notably, passive low-pass filtering (LPF) provides insufficient robustness. TTC, the most relevant baseline, yields only 24.5% accuracy because maximizing divergence without a reliable anchor causes embeddings to drift from the semantic manifold. In contrast, CSR effectively anchors the optimization, achieving **58.1%** robust accuracy—surpassing the strongest baseline by ↑ 6.9%—with a negligible 0.7% clean accuracy drop.

Results under Stronger Attacks. To rigorously evaluate defense stability, we escalate the threat model to include 50-step PGD and the stronger AutoAttack (AA) with an

Table 5. Comparison of zero-shot classification accuracy on CLIP-B/32 and CLIP-L/14 under 10-step PGD ($\ell_\infty = 1/255$).

Method	CLIP-B/32						CLIP-L/14									
	General		FG		Scene		Domain		General		FG		Scene		Domain	
	clean	rob.	clean	rob.	clean	rob.	clean	rob.	clean	rob.	clean	rob.	clean	rob.	clean	rob.
CLIP	76.7	4.0	71.8	0.3	38.8	0.4	35.9	6.6	83.7	4.0	84.2	0.3	45.3	0.2	46.8	0.3
TeCoA	60.3	58.9	35.1	32.4	17.2	17.8	25.1	25.6	73.3	72.9	45.6	41.6	26.5	25.3	30.6	31.4
FARE	59.6	58.4	52.6	48.3	23.2	22.3	27.7	28.0	75.3	74.6	63.9	57.6	32.7	32.5	32.7	32.4
R-TPT	72.9	41.9	71.4	45.4	38.7	29.6	35.7	27.2	84.2	76.8	83.5	70.3	47.1	37.5	42.4	37.3
LPF	74.8	38.0	62.0	18.9	36.2	11.3	33.7	17.4	84.0	66.9	78.8	51.7	44.2	26.2	44.5	28.5
HD	76.0	15.9	68.6	4.9	35.1	3.1	35.1	13.6	82.7	38.3	79.7	9.3	43.0	6.2	44.2	15.9
Anti-Adv	75.3	39.1	70.3	12.6	37.3	7.0	33.2	19.9	82.5	67.9	82.4	48.0	45.2	22.0	43.5	30.9
TTE	77.5	47.3	68.6	27.9	39.3	9.6	36.8	19.3	86.1	58.5	81.6	32.3	47.8	12.2	43.7	23.6
TTC	74.5	43.5	66.5	27.5	32.9	17.5	34.2	22.4	80.5	33.3	70.3	39.7	35.1	19.7	42	15.5
CSR	76.1 ^{40.6}	50.9 ^{46.9}	71.4^{40.4}	41.1 ^{40.8}	38.3 ^{10.5}	30.2^{29.8}	35.8^{40.2}	29.7^{23.1}	82.2 ^{41.5}	77.5^{47.3}	83.5^{40.7}	73.6^{47.3}	44.2 ^{41.1}	45.8^{45.6}	45.6^{41.2}	45.9^{45.6}

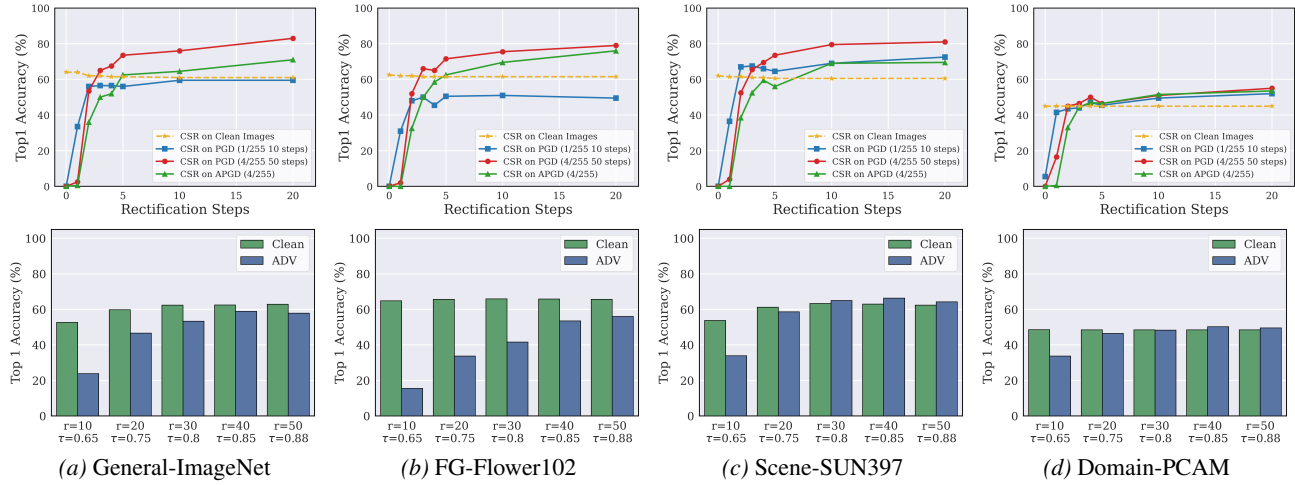

 Figure 5. Ablation study on the rectification steps N , the Gaussian filter radius r , and the detection threshold τ . More in Appendix G

Table 6. Ablation study on CSR framework.

Loss Terms	Greedy	General	FG	Scene	Domain
Attraction	Clean	Rob.	Clean	Rob.	Clean
Repulsion	Clean	Rob.	Clean	Rob.	Clean
✓	✓	78.2	44.7	74.5	33.3
✓	✓	79.3	51.6	75.8	33.8
✓	✓	78.6	68.5	74.7	65.1
✓	✓	78.7	69.8	74.8	65.3

Table 7. Results on various vision tasks. (mIoU/Accuracy)

Method	Segmentation		Captioning		VQA	
	Clean	Rob.	Clean	Rob.	Clean	Rob.
Origin Model	37.7	20.8	100.0	21.3	100.0	22.6
+TTC defense	35.1	21.9	87.4	24.1	87.7	27.3
+CSR defense	37.5 ^{40.2}	37.5 ^{46.7}	99.2^{40.8}	64.3^{43.0}	98.7^{41.3}	65.6^{43.0}

increased budget of $\ell_\infty = 4/255$. As detailed in Table 2, CSR demonstrates exceptional resilience, consistently outperforming baselines while preserving clean accuracy. Adversarial fine-tuning methods (e.g., TeCoA, FARE) exhibit commendable robustness under strong attacks, validating the efficacy of weight modification; however, this comes at the cost of severe degradation in benign performance. In contrast, other test-time defenses crumble under increased adversarial pressure. Methods like TTC, Anti-Adv, and HD exhibit near-zero robustness against AA, revealing their

fragility. Even the computationally expensive R-TPT struggles to maintain stability (dropping to 28.4% on General). Conversely, CSR effectively rectifies the adversarial manifold, achieving **66.4%** average accuracy under AA—a significant **18.1%** improvement over the best test-time baseline—while preserving original zero-shot capabilities.

Results under Different Attack Objectives. To validate the versatility of CSR, we extend our evaluation to a broad spectrum of adversarial objectives (Details in Appendix E.2), including Cross-Modal attacks (disrupting image-text alignment), Targeted attacks (forcing specific misclassification), and Label-free attacks (maximizing visual feature deviation). As presented in Table 4, CSR exhibits consistent superiority across all scenarios. Notably, in Cross-Modal settings, CSR significantly outperforms FARE by approximately **14%** under PGD attacks, while maintaining high benign accuracy. These confirm that CSR functions as a generalized defense, capable of effectively rectifying adversarial perturbations agnostic to the attacker’s specific optimization strategy.

Inference Efficiency Analysis. Table 3 compares the inference latency across different defense methods. While R-TPT achieves competitive robustness, it incurs high computational costs (176.33 ms) due to complex image transfor-

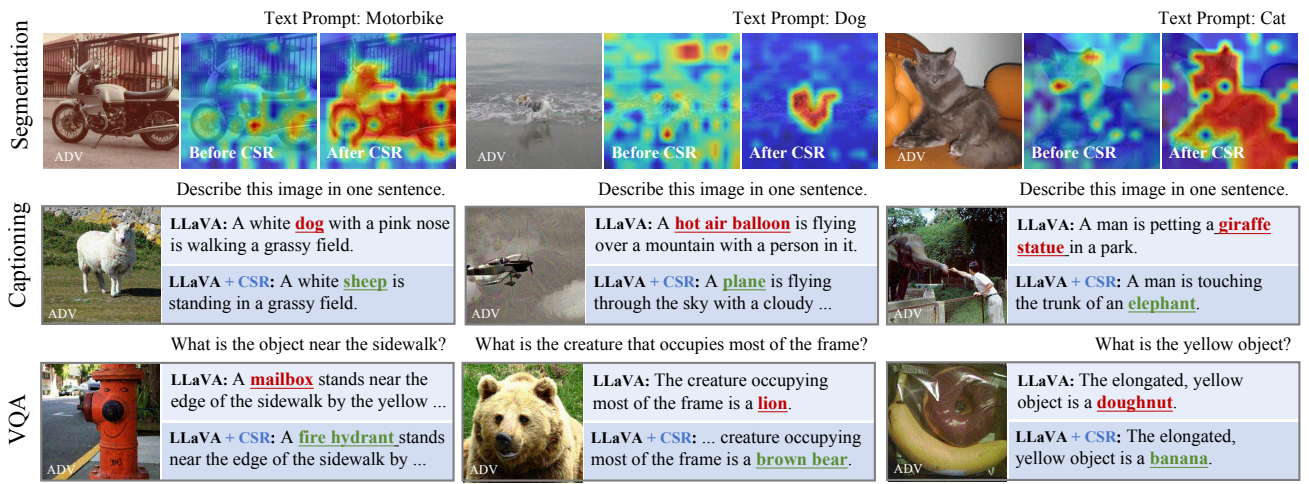


Figure 6. Visualization of Semantic Segmentation (top), Image Captioning, and Visual Question Answering (bottom). More in Appendix H.

mations and prompt optimization. In contrast, CSR demonstrates superior efficiency. This confirms that CSR achieves the optimal trade-off between performance and computational cost, making it suitable for real-time deployment.

Results on Different Backbones. To validate the architectural universality of CSR, we extend our evaluation to CLIP-ViT-B/32 and CLIP-ViT-L/14. As shown in Table 5, the observations remain consistent with those on ViT-B/16. CSR demonstrates superior scalability, achieves state-of-the-art robustness while preserving high clean accuracy.

Results on Various Vision Tasks. Most existing test-time defenses are inherently task-specific, rendering them inapplicable to complex downstream scenarios. To demonstrate the universality of CSR, we subject the CLIP-based Zero-Shot Segmentation (Lan et al., 2024) to PGD attacks ($\ell_\infty = 4/255$) and evaluate the robustness of LLaVA on Captioning and VQA tasks against strong V-Attack (Nie et al., 2025) ($\ell_\infty = 16/255$). Detailed experiment settings are provided in Appendix E.3. As reported in Table 7, while the generic method TTC fails to provide an effective defense, yielding negligible improvements, CSR serves as a robust shield for various downstream applications. It remarkably restores segmentation performance (boosting mIoU by $\uparrow 16.7\%$) and successfully mitigates adversarial attacks in LLaVA, improving accuracy by $\uparrow 43\%$ on both Captioning and VQA tasks. These quantitative gains are corroborated qualitatively in Figure 6. In the top row, CSR rectifies corrupted segmentation masks to recover fine-grained structural details; in the bottom row, it effectively purifies the visual input, correcting model errors (e.g., rectifying “dog” back to “sheep”) and ensuring accurate reasoning. This confirms that CSR functions as a versatile, plug-and-play module that promotes broad security across the CLIP ecosystem (e.g., Large Vision-Language Models).

5.3 Ablation

The CSR Framework. We validate the contribution of each component within our proposed framework, as summarized

in Table 6. The results indicate that the Attraction and Repulsion terms are mutually reinforcing. Employing either term in isolation yields suboptimal robustness. However, their joint application leads to a substantial performance leap (e.g., boosting robustness on General datasets from **51.6%** to **69.8%**). Furthermore, the incorporation of the Greedy Selection strategy consistently optimizes the results.

Hyperparameter Sensitivity. Figure 5 illustrates CSR’s sensitivity to the rectification steps N , the Gaussian filter radius r , and the detection threshold τ . Specifically, increasing N consistently enhances robustness but scales up computational overhead; we find $N = 3$ strikes an optimal balance between efficacy and efficiency. Remarkably, under strong attacks ($\ell_\infty = 4/255$), the post-rectification accuracy even surpasses the clean accuracy. This counterintuitive phenomenon suggests that adversarial examples implicitly encode directional priors of the decision boundary, which CSR leverages to bolster robustness. Notably, a small radius (e.g., $r = 10$) yields suboptimal robustness results. We attribute this to excessive information loss in the anchor, which weakens semantic guidance and hinders adversarial rectification. However, benign samples remain largely unaffected due to our input-adaptive gating mechanism.

6 Conclusion

In this work, we deconstruct the vulnerability of CLIP through the lens of frequency analysis. Guided by these insights, we introduce Contrastive Spectral Rectification (CSR), a novel test-time defense that strategically leverages contrastive anchors for both adversarial detection and purification. Given that CLIP serves as the foundational “eyes” of modern multimodal systems, ensuring its security is paramount. As an efficient, effective, and universal framework, CSR not only fortifies the visual encoder itself but also provides a scalable blueprint for enhancing the robustness of the broader ecosystem of vision-language tasks, paving the way for more reliable and secure artificial intelligence.

References

Abdul Samad, J., Gani, M. H., Hussein, N., Khattak, M. U., Naseer, M. M., Shahbaz Khan, F., and Khan, S. H. Align your prompts: Test-time prompting with distribution alignment for zero-shot generalization. *Advances in Neural Information Processing Systems*, 36: 80396–80413, 2023.

Alfarra, M., Pérez, J. C., Thabet, A., Bibi, A., Torr, P. H., and Ghanem, B. Combating adversaries with anti-adversaries. In *Proceedings of the AAAI Conference on Artificial Intelligence*, volume 36, pp. 5992–6000, 2022.

Awais, M., Naseer, M., Khan, S., Anwer, R. M., Cholakkal, H., Shah, M., Yang, M.-H., and Khan, F. S. Foundation models defining a new era in vision: a survey and outlook. *IEEE Transactions on Pattern Analysis and Machine Intelligence*, 2025.

Bai, J., Bai, S., Yang, S., Wang, S., Tan, S., Wang, P., Lin, J., Zhou, C., and Zhou, J. Qwen-vl: A versatile vision-language model for understanding, localization, text reading, and beyond. *arXiv preprint arXiv:2308.12966*, 2023.

Bossard, L., Guillaumin, M., and Van Gool, L. Food-101—mining discriminative components with random forests. In *European conference on computer vision*, pp. 446–461. Springer, 2014.

Chen, K., Muyang, L., Li, G., Zhang, S., Guo, S., and Zhang, T. Trust-vlm: Thorough red-teaming for uncovering safety threats in vision-language models. In *Forty-second International Conference on Machine Learning*, 2025a.

Chen, L., Chen, Y., Ouyang, Z., Dou, H., Zhang, Y., and Sang, H. Boosting adversarial transferability in vision-language models via multimodal feature heterogeneity. *Scientific Reports*, 15(1):7366, 2025b.

Chen, M., Zhang, B., Han, Z., Jiang, W., Wang, Y., Feng, S., Du, Y., and Bao, B. Test-time selective adaptation for uni-modal distribution shift in multi-modal data. In *ICML*, 2025c.

Chen, Z., Wu, J., Wang, W., Su, W., Chen, G., Xing, S., Zhong, M., Zhang, Q., Zhu, X., Lu, L., et al. Internvl: Scaling up vision foundation models and aligning for generic visual-linguistic tasks. In *Proceedings of the IEEE/CVF conference on computer vision and pattern recognition*, pp. 24185–24198, 2024.

Cimpoi, M., Maji, S., Kokkinos, I., Mohamed, S., and Vedaldi, A. Describing textures in the wild. In *Proceedings of the IEEE conference on computer vision and pattern recognition*, pp. 3606–3613, 2014.

Coates, A., Ng, A., and Lee, H. An analysis of single-layer networks in unsupervised feature learning. In *Proceedings of the fourteenth international conference on artificial intelligence and statistics*, pp. 215–223. JMLR Workshop and Conference Proceedings, 2011.

Croce, F. and Hein, M. Reliable evaluation of adversarial robustness with an ensemble of diverse parameter-free attacks. In *International conference on machine learning*, pp. 2206–2216. PMLR, 2020.

Deng, J., Dong, W., Socher, R., Li, L.-J., Li, K., and Fei-Fei, L. Imagenet: A large-scale hierarchical image database. In *2009 IEEE conference on computer vision and pattern recognition*, pp. 248–255. Ieee, 2009.

Deng, J., Li, J., Zhao, Z., and Wang, S. Fpt-noise: Dynamic scene-aware counterattack for test-time adversarial defense in vision-language models. *arXiv preprint arXiv:2510.20856*, 2025.

Ding, N., Qin, Y., Yang, G., Wei, F., Yang, Z., Su, Y., Hu, S., Chen, Y., Chan, C.-M., Chen, W., et al. Parameter-efficient fine-tuning of large-scale pre-trained language models. *Nature machine intelligence*, 5(3):220–235, 2023.

Dong, H., Chatzi, E. N., and Fink, O. Towards robust multimodal open-set test-time adaptation via adaptive entropy-aware optimization. In *ICLR*. OpenReview.net, 2025a.

Dong, J., Koniusz, P., Feng, L., Zhang, Y., Zhu, H., Liu, W., Qu, X., and Ong, Y.-S. Robustifying zero-shot vision language models by subspaces alignment. In *Proceedings of the IEEE/CVF International Conference on Computer Vision*, pp. 21037–21047, 2025b.

Dong, J., Koniusz, P., Zhang, Y., Zhu, H., Liu, W., Qu, X., and Ong, Y.-S. Improving zero-shot adversarial robustness in vision-language models by closed-form alignment of adversarial path simplices. In *Forty-second International Conference on Machine Learning*, 2025c.

Dong, Y., Chen, H., Chen, J., Fang, Z., Yang, X., Zhang, Y., Tian, Y., Su, H., and Zhu, J. How robust is google’s bard to adversarial image attacks? *arXiv preprint arXiv:2309.11751*, 2023.

Everingham, M., Van Gool, L., Williams, C. K. I., Winn, J., and Zisserman, A. The pascal visual object classes (VOC) challenge. *International Journal of Computer Vision (IJCV)*, 88(2):303–338, 2010.

Fang, H., Kong, J., Yu, W., Chen, B., Li, J., Xia, S., and Xu, K. One perturbation is enough: On generating universal adversarial perturbations against vision-language pre-training models. *CoRR*, abs/2406.05491, 2024.

Fei-Fei, L., Fergus, R., and Perona, P. Learning generative visual models from few training examples: An incremental bayesian approach tested on 101 object categories. In *2004 conference on computer vision and pattern recognition workshop*, pp. 178–178. IEEE, 2004.

Gao, S., Jia, X., Ren, X., Tsang, I. W., and Guo, Q. Boosting transferability in vision-language attacks via diversification along the intersection region of adversarial trajectory. In *ECCV (57)*, volume 15115 of *Lecture Notes in Computer Science*, pp. 442–460. Springer, 2024.

Griffin, G., Holub, A., Perona, P., et al. Caltech-256 object category dataset. Technical report, Technical Report 7694, California Institute of Technology Pasadena, 2007.

Guo, Q., Pang, S., Jia, X., and Guo, Q. Efficiently adversarial examples generation for visual-language models under targeted transfer scenarios using diffusion models. *CoRR*, 2024.

Han, J. and Hwang, W. D-tpt: Dimensional entropy maximization for calibrating test-time prompt tuning in vision-language models. *arXiv preprint arXiv:2510.09473*, 2025.

Han, Z., Gao, C., Liu, J., Zhang, J., and Zhang, S. Q. Parameter-efficient fine-tuning for large models: A comprehensive survey. *Trans. Mach. Learn. Res.*, 2024, 2024.

He, B., Jia, X., Liang, S., Lou, T., Liu, Y., and Cao, X. Sa-attack: Improving adversarial transferability of vision-language pre-training models via self-augmentation. *arXiv preprint arXiv:2312.04913*, 2023.

He, X. et al. Anyattack: Towards large-scale self-supervised adversarial attacks on vision-language models. In *Proceedings of the IEEE/CVF Conference on Computer Vision and Pattern Recognition (CVPR)*, 2025.

Helber, P., Bischke, B., Dengel, A., and Borth, D. Eurosat: A novel dataset and deep learning benchmark for land use and land cover classification. *IEEE Journal of Selected Topics in Applied Earth Observations and Remote Sensing*, 12(7):2217–2226, 2019.

Hossain, M. Z. and Imteaj, A. Securing vision-language models with a robust encoder against jailbreak and adversarial attacks. In *2024 IEEE International Conference on Big Data (BigData)*, pp. 6250–6259. IEEE, 2024.

Hu, A., Gu, J., Pinto, F., Kamnitsas, K., and Torr, P. As firm as their foundations: Can open-sourced foundation models be used to create adversarial examples for downstream tasks? *CoRR*, abs/2403.12693, 2024.

Hu, J., Zhang, Z., Chen, G., Wen, X., Shuai, C., Luo, W., Xiao, B., Li, Y., and Tan, M. Test-time learning for large language models. In *ICML*, 2025.

Hussein, N., Shamshad, F., Naseer, M., and Nandakumar, K. Promptsmooth: Certifying robustness of medical vision-language models via prompt learning. In *International Conference on Medical Image Computing and Computer-Assisted Intervention*, pp. 698–708. Springer, 2024.

Ilyas, A., Santurkar, S., Tsipras, D., Engstrom, L., Tran, B., and Madry, A. Adversarial examples are not bugs, they are features. In *Advances in Neural Information Processing Systems (NeurIPS)*, volume 32, 2019.

Jia, X., Gao, S., Qin, S., Pang, T., Du, C., Huang, Y., Li, X., Li, Y., Li, B., and Liu, Y. Adversarial attacks against closed-source mllms via feature optimal alignment. *arXiv preprint arXiv:2505.21494*, 2025.

Jing, L., Wu, Y., Yang, J., Chen, Y., and Tian, Q. Vision-language models for vision tasks: A survey. *IEEE Transactions on Pattern Analysis and Machine Intelligence (TPAMI)*, 2024.

Krause, J., Stark, M., Deng, J., and Fei-Fei, L. 3d object representations for fine-grained categorization. In *Proceedings of the IEEE international conference on computer vision workshops*, pp. 554–561, 2013.

Krizhevsky, A., Hinton, G., et al. Learning multiple layers of features from tiny images. *Technical Report, University of Toronto*, 2009.

Lan, M., Chen, C., Ke, Y., Wang, X., Feng, L., and Zhang, W. Clearclip: Decomposing clip representations for dense vision-language inference. In *European Conference on Computer Vision*, pp. 143–160. Springer, 2024.

Li, L., Guan, H., Qiu, J., and Spratling, M. One prompt word is enough to boost adversarial robustness for pre-trained vision-language models. In *Proceedings of the IEEE/CVF Conference on Computer Vision and Pattern Recognition*, pp. 24408–24419, 2024a.

Li, X., Zhang, W., Liu, Y., Hu, Z., Zhang, B., and Hu, X. Language-driven anchors for zero-shot adversarial robustness. In *Proceedings of the IEEE/CVF Conference on Computer Vision and Pattern Recognition*, pp. 24686–24695, 2024b.

Li, Z., Zhao, X., Wu, D.-D., Cui, J., and Shen, Z. A frustratingly simple yet highly effective attack baseline: Over 90success rate against the strong black-box models of gpt-4.5/4o/o1. *arXiv preprint arXiv:2503.10635*, 2025.

Lin, T.-Y., Maire, M., Belongie, S., Hays, J., Perona, P., Ramanan, D., Dollár, P., and Zitnick, C. L. Microsoft COCO: Common objects in context. In *European Conference on Computer Vision (ECCV)*, pp. 740–755. Springer, 2014.

Liu, H., Li, C., Wu, Q., and Lee, Y. J. Visual instruction tuning. *Advances in neural information processing systems*, 36:34892–34916, 2023.

Liu, Y., Ouyang, X., and Cui, X. Gleam: Enhanced transferable adversarial attacks for vision-language pre-training models via global-local transformations. In *Proceedings of the IEEE/CVF International Conference on Computer Vision*, pp. 1665–1674, 2025.

Lu, D., Wang, Z., Wang, T., Guan, W., Gao, H., and Zheng, F. Set-level guidance attack: Boosting adversarial transferability of vision-language pre-training models. In *Proceedings of the IEEE/CVF International Conference on Computer Vision*, pp. 102–111, 2023.

Lu, H., Liu, W., Zhang, B., Wang, B., Dong, K., Liu, B., Sun, J., Ren, T., Li, Z., Yang, H., et al. Deepseek-vl: towards real-world vision-language understanding. *arXiv preprint arXiv:2403.05525*, 2024.

Ma, X., Gao, Y., Wang, Y., Wang, R., Wang, X., Sun, Y., Ding, Y., Xu, H., Chen, Y., Zhao, Y., et al. Safety at scale: A comprehensive survey of large model safety. *arXiv preprint arXiv:2502.05206*, 2025.

Madry, A., Makelov, A., Schmidt, L., Tsipras, D., and Vladu, A. Towards deep learning models resistant to adversarial attacks. *arXiv preprint arXiv:1706.06083*, 2017.

Maji, S., Rahtu, E., Kannala, J., Blaschko, M., and Vedaldi, A. Fine-grained visual classification of aircraft. *arXiv preprint arXiv:1306.5151*, 2013.

Mao, C., Geng, S., Yang, J., Wang, X., and Vondrick, C. Understanding zero-shot adversarial robustness for large-scale models. In *ICLR*, 2023.

Naseer, M. M., Ranasinghe, K., Khan, S. H., Hayat, M., Shahbaz Khan, F., and Yang, M.-H. Intriguing properties of vision transformers. *Advances in Neural Information Processing Systems*, 34:23296–23308, 2021.

Nie, S., Zhang, J., Yan, J., Shan, S., and Chen, X. V-attack: Targeting disentangled value features for controllable adversarial attacks on l1lms. *arXiv preprint arXiv:2511.20223*, 2025.

Nilsback, M.-E. and Zisserman, A. Automated flower classification over a large number of classes. In *2008 Sixth Indian conference on computer vision, graphics & image processing*, pp. 722–729. IEEE, 2008.

Noever, D. A. and Noever, S. E. M. Reading isn’t believing: Adversarial attacks on multi-modal neurons. *arXiv preprint arXiv:2103.10480*, 2021.

Parkhi, O. M., Vedaldi, A., Zisserman, A., and Jawahar, C. Cats and dogs. In *2012 IEEE conference on computer vision and pattern recognition*, pp. 3498–3505. IEEE, 2012.

Pérez, J. C., Alfarra, M., Jeanneret, G., Rueda, L., Thabet, A., Ghanem, B., and Arbeláez, P. Enhancing adversarial robustness via test-time transformation ensembling. In *Proceedings of the IEEE/CVF International Conference on Computer Vision*, pp. 81–91, 2021.

Qian, Y., Yu, Q., Bao, Q., Ji, S., Wang, W., Wang, B., Gu, Z., and Lei, Z. A multimodal adversarial attack method via frequency domain enhancement and fine-grained cross-modal guidance. *IEEE Transactions on Dependable and Secure Computing*, 2025.

Radford, A., Kim, J. W., Hallacy, C., Ramesh, A., Goh, G., Agarwal, S., Sastry, G., Askell, A., Mishkin, P., Clark, J., et al. Learning transferable visual models from natural language supervision. In *International conference on machine learning*, pp. 8748–8763. PMLR, 2021.

Reyes-Amezcua, I., Ochoa-Ruiz, G., and Mendez-Vazquez, A. Enhancing image classification robustness through adversarial sampling with delta data augmentation (dda). In *Proceedings of the IEEE/CVF Conference on Computer Vision and Pattern Recognition*, pp. 274–283, 2024.

Schlarmann, C., Singh, N. D., Croce, F., and Hein, M. Robust clip: Unsupervised adversarial fine-tuning of vision embeddings for robust large vision-language models. *ICML*, 2024.

Shen, S., Li, L. H., Tan, H., Bansal, M., Rohrbach, A., Chang, K., Yao, Z., and Keutzer, K. How much can CLIP benefit vision-and-language tasks? In *ICLR*, 2022.

Sheng, L., Liang, J., Wang, Z., and He, R. R-tpt: Improving adversarial robustness of vision-language models through test-time prompt tuning. In *Proceedings of the Computer Vision and Pattern Recognition Conference*, pp. 29958–29967, 2025.

Shu, M., Nie, W., Huang, D.-A., Yu, Z., Goldstein, T., Anandkumar, A., and Xiao, C. Test-time prompt tuning for zero-shot generalization in vision-language models. *Advances in Neural Information Processing Systems*, 35: 14274–14289, 2022.

Su, L. and Balogh, A. Atac: Augmentation-based test-time adversarial correction for clip. *arXiv preprint arXiv:2511.17362*, 2025.

Sui, Y., Huang, W., Yang, W., Zhao, C., Ren, J., and Wang, J. Robust clip-guided deep thinking: A two-stage optimization strategy for enhancing adversarial robustness

and reliability in lvlms. In *ICASSP 2025-2025 IEEE International Conference on Acoustics, Speech and Signal Processing (ICASSP)*, pp. 1–5. IEEE, 2025.

Tong, B., Lai, H., Pan, Y., and Yin, J. On the zero-shot adversarial robustness of vision-language models: A truly zero-shot and training-free approach. In *Proceedings of the Computer Vision and Pattern Recognition Conference*, pp. 19921–19930, 2025.

Veeling, B. S., Linmans, J., Winkens, J., Cohen, T., and Welling, M. Rotation equivariant cnns for digital pathology. In *International Conference on Medical image computing and computer-assisted intervention*, pp. 210–218. Springer, 2018.

Wang, H., Dong, K., Zhu, Z., Qin, H., Liu, A., Fang, X., Wang, J., and Liu, X. Transferable multimodal attack on vision-language pre-training models. In *2024 IEEE Symposium on Security and Privacy (SP)*, pp. 1722–1740. IEEE, 2024a.

Wang, S., Zhang, J., Yuan, Z., and Shan, S. Pre-trained model guided fine-tuning for zero-shot adversarial robustness. In *Proceedings of the IEEE/CVF conference on computer vision and pattern recognition*, pp. 24502–24511, 2024b.

Wang, X., Chen, K., Zhang, J., Chen, J., and Ma, X. Tapt: Test-time adversarial prompt tuning for robust inference in vision-language models. In *Proceedings of the Computer Vision and Pattern Recognition Conference*, pp. 19910–19920, 2025a.

Wang, Y., Hu, W., Dong, Y., Zhang, H., Su, H., and Hong, R. Exploring transferability of multimodal adversarial samples for vision-language pre-training models with contrastive learning. *IEEE Transactions on Multimedia*, 2025b.

Wang, Z., Li, X., Zhu, H., and Xie, C. Revisiting adversarial training at scale. In *Proceedings of the IEEE/CVF Conference on Computer Vision and Pattern Recognition*, pp. 24675–24685, 2024c.

Wang, Z., Ding, N., and Mahanti, A. Learning robust vision-language models from natural latent spaces. In *The Thirty-ninth Annual Conference on Neural Information Processing Systems*, 2025c.

Wu, B., Pan, H., Shen, L., Gu, J., Zhao, S., Li, Z., Cai, D., He, X., and Liu, W. Attacking adversarial attacks as a defense. *arXiv preprint arXiv:2106.04938*, 2021.

Xiao, J., Hays, J., Ehinger, K. A., Oliva, A., and Torralba, A. Sun database: Large-scale scene recognition from abbey to zoo. In *2010 IEEE computer society conference on computer vision and pattern recognition*, pp. 3485–3492. IEEE, 2010.

Xing, S., Zhao, Z., and Sebe, N. Clip is strong enough to fight back: Test-time counterattacks towards zero-shot adversarial robustness of clip. In *Proceedings of the Computer Vision and Pattern Recognition Conference*, pp. 15172–15182, 2025.

Yin, Z., Ye, M., Zhang, T., Du, T., Zhu, J., Liu, H., Chen, J., Wang, T., and Ma, F. Vlattack: Multimodal adversarial attacks on vision-language tasks via pre-trained models. *Advances in Neural Information Processing Systems*, 36: 52936–52956, 2023.

Zhai, K., Chen, S., Ma, X., and Jiang, Y.-G. Fedapt: Federated adversarial prompt tuning for vision-language models. In *Proceedings of the 33rd ACM International Conference on Multimedia*, pp. 4310–4318, 2025.

Zhang, J., Yi, Q., and Sang, J. Towards adversarial attack on vision-language pre-training models. In *Proceedings of the 30th ACM International Conference on Multimedia*, pp. 5005–5013, 2022.

Zhang, J., Ma, X., Wang, X., Qiu, L., Wang, J., Jiang, Y.-G., and Sang, J. Adversarial prompt tuning for vision-language models. In *European conference on computer vision*, pp. 56–72. Springer, 2024a.

Zhang, J., Ye, J., Ma, X., Li, Y., Yang, Y., Sang, J., and Yeung, D.-Y. Anyattack: Towards large-scale self-supervised generation of targeted adversarial examples for vision-language models. *arXiv e-prints*, pp. arXiv-2410, 2024b.

Zhang, J., Ye, J., Ma, X., Li, Y., Yang, Y., Chen, Y., Sang, J., and Yeung, D.-Y. Anyattack: Towards large-scale self-supervised adversarial attacks on vision-language models. In *Proceedings of the Computer Vision and Pattern Recognition Conference*, pp. 19900–19909, 2025a.

Zhang, M., Bi, K., Chen, W., Guo, J., and Cheng, X. Clipure: Purification in latent space via CLIP for adversarially robust zero-shot classification. In *ICLR. OpenReview.net*, 2025b.

Zhang, P., Huang, Z., and Bai, G. Universal adversarial perturbations for vision-language pre-trained models. In *SIGIR*, pp. 862–871. ACM, 2024c.

Zhao, Y., Pang, T., Du, C., Yang, X., Li, C., Cheung, N., and Lin, M. On evaluating adversarial robustness of large vision-language models. In *NeurIPS*, 2023.

Zhao, Y., Pang, T., Du, C., Yang, X., Li, C.-Y., Cheung, N.-M., and Lin, M. On the robustness of large multimodal models against image adversarial attacks. In *Proceedings of the IEEE/CVF Conference on Computer Vision and Pattern Recognition (CVPR)*, 2024.

Zhou, S., Yin, M., Sun, L., Yang, S., Xie, D., and Zhu, J. Training-free test-time adaptation via shape and style guidance for vision-language models. In *The Thirty-ninth Annual Conference on Neural Information Processing Systems*, 2025.

Zhou, W., Bai, S., Mandic, D. P., Zhao, Q., and Chen, B. Revisiting the adversarial robustness of vision language models: a multimodal perspective. *arXiv preprint arXiv:2404.19287*, 2024a.

Zhou, Y., Xia, X., Lin, Z., Han, B., and Liu, T. Few-shot adversarial prompt learning on vision-language models. *Advances in Neural Information Processing Systems*, 37: 3122–3156, 2024b.

Zhou, Z., Hu, S., Li, M., Zhang, H., Zhang, Y., and Jin, H. Advclip: Downstream-agnostic adversarial examples in multimodal contrastive learning. In *Proceedings of the 31st ACM International Conference on Multimedia*, pp. 6311–6320, 2023.

Zhu, X., Zhu, B., Wang, S., Zhao, K., and Zhang, H. Enhancing clip robustness via cross-modality alignment. *The Thirty-ninth Annual Conference on Neural Information Processing Systems*, 2025.

Ziyadinov, V. and Tereshonok, M. Low-pass image filtering to achieve adversarial robustness. *Sensors*, 23(22):9032, 2023.

Appendix: Table of Contents

Section A	Related Work on Adversarial Attacks	14
Section B	Theoretical Analysis of Gradient Conflict	14
Section C	Disparity in Feature Consistency	15
Section D	CSR Detection AUC on 15 Datasets	15
Section E	Additional Implementation Details	15
	Attacks with Different Objectives	15
	CSR on Various Vision Tasks	16
Section F	Results on CLIP ViT-L/14 and ViT-B/32	17
Section G	Ablation of Rectification Steps	17
Section H	Additional Visualization	17

A Related Work on Adversarial Attacks

Adversarial Attacks on VLMs. Current research on VLM vulnerabilities can be broadly categorized into white-box optimization and black-box transfer-based paradigms (Qian et al., 2025; Chen et al., 2025b; Liu et al., 2025; Zhang et al., 2025a). In the white-box setting, Typographical Attacks (Noever & Noever, 2021) exposed CLIP’s “read first, look later” bias via visible text patches. Optimization-based strategies subsequently emerged to disrupt cross-modal alignment: Co-Attack (Zhang et al., 2022) pioneered the joint perturbation of both visual and textual inputs, while AdvCLIP (Zhou et al., 2023) explored universal perturbations capable of deceiving diverse downstream tasks. To address black-box transferability, recent works predominantly leverage augmentation and cross-modal priors. Specifically, SGA (Lu et al., 2023), SA-Attack (He et al., 2023), and DIRAT (Gao et al., 2024) enhance transferability via set-level augmentations. VLP-Attack (Wang et al., 2025b) utilizes contrastive objectives to generate transferable examples, while TMM (Wang et al., 2024a) and VLATTACK (Yin et al., 2023) exploit modality-consistent features and combined multi-modal perturbations. Additionally, PRM (Hu et al., 2024) specifically targets vulnerabilities in downstream applications. C-PGC (Fang et al., 2024) pioneers this line of research by optimizing Universal Adversarial Perturbations (UAPs) via contrastive learning, and ETU (Zhang et al., 2024c) further elevates their potency through global optimization and mix-based data augmentation.

Adversarial Attacks on LVLMs. A critical vulnerability in Large Vision-Language Models (LVLMs)—such as LLaVA (Liu et al., 2023), Qwen-VL (Bai et al., 2023), InternVL (Chen et al., 2024), and DeepseekVL (Lu et al., 2024)—stems from their vision encoders. This architectural commonality allows attackers to utilize CLIP as a surrogate model to craft transfer-based attacks (Ma et al., 2025). For instance, AttackBard (Dong et al., 2023), AttackVLM (Zhao et al., 2023), M-Attack (Li et al., 2025), FOA-Attack (Jia et al., 2025), and V-Attack (Nie et al., 2025) demonstrate

that adversarial examples generated from CLIP can effectively mislead closed-source models. Generator-based strategies leverage generative priors: AdvDiffVLM (Guo et al., 2024) employs diffusion models with gradient estimation to synthesize adversarial images, while AnyAttack (Zhang et al., 2024b) introduces a self-supervised contrastive framework to generate label-free adversarial examples capable of compromising diverse tasks.

Given that CLIP-based encoders act as the cornerstone for modern multimodal systems, their adversarial fragility constitutes a critical security bottleneck. Therefore, developing robust defenses for these foundational models is pivotal to securing the broader landscape of intelligent systems against adversarial threats. This motivates our CSR defense.

B Theoretical Analysis of Gradient Conflict

In this section, we analyze the geometric relationship between the gradient of the proposed spectral consistency objective and the direction of adversarial perturbations. By employing a local linearization of the encoder, we demonstrate that the optimization of our auxiliary loss generates a restorative force that specifically counters high-frequency noise aligned with the model’s feature sensitivity.

Problem Setup. Let $f : \mathbb{R}^d \rightarrow \mathbb{R}^k$ be the encoder, and $\mathbf{G} \in \mathbb{R}^{d \times d}$ be a symmetric, linear low-pass filter (e.g., Gaussian). We define the high-pass projection operator as $\mathbf{P} = \mathbf{I} - \mathbf{G}$. The consistency loss is given by:

$$\mathcal{L}_{sim}(\mathbf{x}) = \frac{1}{2} \|f(\mathbf{x}) - f(\mathbf{G}\mathbf{x})\|_2^2. \quad (8)$$

Local Linearization. Since natural images are dominated by low-frequency components, the term $\|\mathbf{x} - \mathbf{G}\mathbf{x}\|_2$ is typically small. We approximate the behavior of f using a first-order Taylor expansion around the smoothed anchor point $\mathbf{G}\mathbf{x}$. Assuming the encoder is locally smooth:

$$f(\mathbf{x}) \approx f(\mathbf{G}\mathbf{x}) + \mathbf{J}(\mathbf{G}\mathbf{x})(\mathbf{x} - \mathbf{G}\mathbf{x}) = f(\mathbf{G}\mathbf{x}) + \mathbf{J}\mathbf{P}\mathbf{x}, \quad (9)$$

where $\mathbf{J} \triangleq \mathbf{J}_f(\mathbf{G}\mathbf{x}) \in \mathbb{R}^{k \times d}$ is the input-output Jacobian evaluated at the smoothed image. Under this approximation, the loss simplifies to a quadratic form in the projected space:

$$\tilde{\mathcal{L}}_{sim}(\mathbf{x}) = \frac{1}{2} \|\mathbf{J}\mathbf{P}\mathbf{x}\|_2^2. \quad (10)$$

Gradient Derivation. We derive the gradient of $\tilde{\mathcal{L}}_{sim}$ with respect to \mathbf{x} . Consistent with the local linearization assumption, we treat the Jacobian \mathbf{J} as a constant linear operator within the neighborhood of \mathbf{x} . Using the symmetry of \mathbf{P} :

$$\nabla_{\mathbf{x}} \tilde{\mathcal{L}}_{sim} \approx \mathbf{P}^T \mathbf{J}^T \mathbf{J} \mathbf{P} \mathbf{x} = \mathbf{P} \mathbf{M} \mathbf{P} \mathbf{x}, \quad (11)$$

where $\mathbf{M} = \mathbf{J}^T \mathbf{J} \in \mathbb{R}^{d \times d}$ is the local metric tensor (or the input-output Jacobian Gram matrix), which characterizes the sensitivity of the feature space to input variations.

Conflict with Adversarial Perturbations. Consider an adversarial example $\mathbf{x}_{adv} = \mathbf{x}_{clean} + \boldsymbol{\delta}$. We analyze the geometric alignment between the defense update direction, $-\nabla_{\mathbf{x}} \tilde{\mathcal{L}}_{sim}$, and the adversarial perturbation $\boldsymbol{\delta}$. While theoretically unbounded, effective perturbations are empirically constrained by the model’s spectral properties. As established in Section 3.2, the model exhibits spectral hypersensitivity in high-frequency bands, incentivizing optimization algorithms to concentrate noise energy in these regions to maximize feature distortion efficiently. Consequently, we observe that perturbations are dominated by high-frequency components ($\mathbf{P}\boldsymbol{\delta} \approx \boldsymbol{\delta}$). Under these conditions, the gradient term is governed by the perturbation: $\mathbf{P}\mathbf{x}_{adv} \approx \mathbf{P}\boldsymbol{\delta}$.

The inner product between the defense restorative force and the perturbation is derived as:

$$\begin{aligned} \langle -\nabla_{\mathbf{x}} \tilde{\mathcal{L}}_{sim}, \boldsymbol{\delta} \rangle &\approx -\boldsymbol{\delta}^\top (\mathbf{P}\mathbf{M}\mathbf{P}\boldsymbol{\delta}) \\ &= -(\mathbf{P}\boldsymbol{\delta})^\top \mathbf{M}(\mathbf{P}\boldsymbol{\delta}) \\ &= -\|\mathbf{J}(\mathbf{P}\boldsymbol{\delta})\|_2^2 \leq 0. \end{aligned} \quad (12)$$

This inequality confirms that the defense optimization strictly opposes the adversarial direction. Crucially, the magnitude of this opposition is scaled by $\|\mathbf{J}(\mathbf{P}\boldsymbol{\delta})\|_2^2$. Since adversarial attacks implicitly align $\mathbf{P}\boldsymbol{\delta}$ with the dominant singular vectors of the Jacobian \mathbf{J} to exploit model vulnerability, our objective generates a counter-force that is maximal precisely along these most sensitive directions. This theoretical finding aligns with our empirical observation that \mathcal{L}_{sim} effectively suppresses the “discriminative shortcuts” in the high-frequency domain.

Geometric Interpretation. This implies that our defense does not merely suppress all high-frequency noise uniformly; rather, it exerts the strongest suppression force on perturbations that lie in the dominant singular vector directions of \mathbf{J} . Since adversarial attacks are specifically constructed to align with these sensitive directions to maximize feature distortion, \mathcal{L}_{sim} inherently targets the most destructive components of $\boldsymbol{\delta}$, providing a theoretically grounded explanation for the defense’s efficacy.

C Disparity in Feature Consistency

In this section, we provide a comprehensive evaluation of feature consistency across a broader range of datasets and attack configurations to reinforce the observations in Section 3.1. We extend our analysis to include:

- General Classification: CIFAR-10/100, STL-10, Caltech-101/256, and ImageNet.
- Fine-Grained Recognition: Oxford Pets, Flowers-102, Food-101, and Stanford Cars.
- Scene Understanding: SUN397 and Country211.
- Specialized Domains: FGVC-Aircraft, EuroSAT, DTD,

and PCAM.

For each dataset, we randomly sample 300 instances and generate adversarial examples (AEs) using 10-step PGD and 30-step AutoAttack under various ℓ_∞ budgets.

D CSR Detection AUC on 15 Datasets

We report the Area Under the Curve (AUC) results for benign and adversarial samples (10-step PGD, $\ell_\infty = 1/255$) across 15 datasets, using the default hyperparameters: Gaussian filter radius $r = 40$ and detection threshold $\tau = 0.85$. As illustrated in Figure 10, the Area Under the ROC curve exceeds **0.95** across all datasets, with a dense concentration between **0.98** and **0.99**. These results demonstrate that the input-adaptive gating mechanism in CSR—derived from the intrinsic properties of CLIP discussed in Section 3—effectively distinguishes between benign and adversarial inputs. Notably, this mechanism incurs minimal computational overhead (Table 3), introducing negligible latency on benign samples (increasing from 3.37ms to 4.16ms), which underscores its practical utility for real-world deployment.

E Additional Details of the Experiment

E.1 Additional Implementation Details

In our experiments, unless otherwise specified, we employ PGD and AutoAttack (specifically the APGD algorithm) under the ℓ_∞ norm constraint. The former serves as a standard benchmark for general evaluation, while the latter provides a more rigorous assessment of robustness under strong attacks. All experiments are conducted on a server equipped with eight NVIDIA GeForce RTX 4090 GPUs.

E.2 Attacks with Different Objectives

To further validate the versatility and robustness of CSR, we extend our evaluation to a broad spectrum of adversarial objectives beyond standard untargeted attacks. For all experiments in this section, we maintain a consistent adversarial budget of $\epsilon = 4/255$ under the ℓ_∞ norm, with the number of attack steps set to $T = 50$. The specific formulations for each objective are detailed as follows:

Cross-Modal Attacks. The objective of cross-modal attacks is to disrupt the inherent semantic alignment between the visual and textual modalities in CLIP’s latent space. We employ PGD and AutoAttack (AA) to minimize the cosine similarity between the perturbed image embedding and its corresponding ground-truth text embedding. The loss function is formulated as:

$$\mathcal{L}_{cm} = \frac{f(\mathbf{x} + \boldsymbol{\delta})^\top g(\mathbf{t}_y)}{\|f(\mathbf{x} + \boldsymbol{\delta})\|_2 \cdot \|g(\mathbf{t}_y)\|_2} = \mathbf{z}'_v^\top \mathbf{z}_{t,y}, \quad (13)$$

where \mathbf{z}'_v denotes the normalized embedding of the adver-

arial image. By minimizing this loss, the attacker forces the visual feature to drift away from its semantic anchor.

Targeted Attacks. In the targeted setting, the attacker aims to steer the model’s prediction toward a specific, incorrect class $y_{target} \neq y$. This objective is more aggressive than untargeted attacks as it requires the perturbation to encode structured, misleading semantic information. We evaluate CSR against three representative targeted strategies:

- **PGD:** The perturbation is optimized by minimizing the cross-entropy loss between the predicted probability distribution and the one-hot encoded target label:

$$\begin{aligned} \mathcal{L}_{tar} &= -\log p(y_{target} \mid \mathbf{x} + \boldsymbol{\delta}) \\ &= -\log \left(\frac{\exp(\tau \cdot \mathbf{z}'_v^\top \mathbf{z}_{t,y_{target}})}{\sum_{j=1}^K \exp(\tau \cdot \mathbf{z}'_v^\top \mathbf{z}_{t,j})} \right), \end{aligned} \quad (14)$$

where $\mathbf{z}'_v = f(\mathbf{x} + \boldsymbol{\delta}) / \|f(\mathbf{x} + \boldsymbol{\delta})\|_2$. This forces the visual feature to align closely with the target class’s text embedding $\mathbf{z}_{t,y_{target}}$.

- **DLR:** Moreover, we utilize the targeted version of the Difference of Logits Ratio (DLR) loss:

$$\mathcal{L}_{tar_dlr} = -\frac{s_y - s_{y_{target}}}{s_{\pi_1} - \frac{1}{2}(s_{\pi_3} + s_{\pi_4})}. \quad (15)$$

Here, $s_i = \mathbf{z}'_v^\top \mathbf{z}_{t,i}$ represents the cosine similarities (logits), and π denotes the descending order of these similarities. This loss specifically penalizes the margin between the ground-truth class y and the target class y_{target} .

- **AutoAttack:** We also employ the targeted version of AutoAttack, which serves as a parameter-free benchmark consisting of multiple iterations of targeted APGD to ensure a reliable evaluation of CSR’s defense ceiling.

Label-free Attacks. This category represents a label-free setting where the attacker lacks access to ground-truth labels or textual prompts. In this scenario, the attacker aims to destroy the model’s representational integrity by maximizing the semantic deviation from the original image. Specifically, we employ PGD and AutoAttack (AA) to minimize the cosine similarity between the perturbed visual embedding and the original, unperturbed embedding:

$$\mathcal{L}_{labfree} = \frac{f(\mathbf{x} + \boldsymbol{\delta})^\top f(\mathbf{x})}{\|f(\mathbf{x} + \boldsymbol{\delta})\|_2 \cdot \|f(\mathbf{x})\|_2} = \mathbf{z}'_v^\top \mathbf{z}_v, \quad (16)$$

where \mathbf{z}_v and \mathbf{z}'_v denote the normalized visual embeddings of the clean and adversarial images, respectively. By minimizing this objective, the attacker pushes the adversarial feature as far as possible from its original position in the latent space. Since these attacks are agnostic to textual guidance, they rely solely on the intrinsic visual features, making them a robust measure of CSR’s ability to rectify samples.

As presented in Table 4, our CSR exhibits consistent superiority across all evaluated scenarios.

E.3 CSR on Various Vision Tasks

Current test-time defense strategies are often restricted to specific tasks, such as classification, which limits their applicability and hinders the advancement of security across broader vision tasks. In contrast, our proposed CSR is task-agnostic and can be widely applied to bolster general visual security. To demonstrate this versatility, we extend our evaluation to three additional tasks: Semantic Segmentation, Image Captioning, and Visual Question Answering (VQA).

For the semantic segmentation task, we conduct experiments using the CLIP-B/16 backbone. Regarding the dataset, we utilize VOC2010, from which we randomly select 3k images to perform evaluation. Adversarial examples are generated via AutoAttack (specifically the APGD algorithm) under an ℓ_∞ constraint of 4/255 for $T = 50$ iterations. Following the unlabeled attack setting, the optimization objective is to push the adversarial features away from the original image embeddings in the latent space. For the segmentation framework, we adopt the training-free strategy proposed in (Lan et al., 2024), which enables zero-shot semantic segmentation leveraging CLIP’s cross-modal capabilities.

For Image Captioning and Visual Question Answering (VQA) tasks, we conduct evaluations using the LLaVA framework. To rigorously assess the rectification efficacy of CSR, adversarial examples are generated via V-Attack (Nie et al., 2025), a state-of-the-art attack strategy for Large Vision-Language Models (LVLMs). Specifically, V-Attack utilizes CLIP-L/14@336px as a surrogate model to produce adversarial perturbations that exhibit high transferability across diverse tasks, models, and prompts. Following the configuration in V-Attack, we set the noise budget to $\ell_\infty = 16/255$ with 200 iterations to ensure a sufficiently strong attack. The evaluation is performed on a subset of 300 samples randomly sampled from the COCO dataset. Since V-Attack targets a specific object within an image per iteration, we employ a Large Language Model (LLM) as the evaluator to determine attack success, strictly adhering to the experimental protocols established in V-Attack.

As reported in Table 7, CSR demonstrates robust performance across all three aforementioned tasks, with nearly negligible degradation in accuracy on benign samples. These results indicate that CSR can extensively bolster the security of various vision tasks, providing a solid foundation and significant implications for future research in adversarial attacks and defenses.

F Results on CLIP ViT-L/14 and ViT-B/32

In this section, we present the fine-grained performance across 16 datasets for CLIP-ViT-L/14 and CLIP-ViT-B/32 backbones in Tables 8 and 9, respectively. As a detailed extension of the main results in Table 5, these evaluations corroborate the architectural universality and scalability of the proposed CSR method, aligning with the findings for ViT-B/16 previously discussed in the main text.

G Ablation of Rectification Steps

As illustrated in Figure 8, we present additional ablation studies on the number of rectification steps N across other datasets. Consistent with the analysis in the main text, increasing N progressively enhances the robustness of CSR, albeit at the cost of higher inference latency.

H Visualization

To complement Table 4 and Figure 6, we provide additional visualization examples in Figure 7.

Table 8. Performance comparison across different dataset types and method categories on CLIP-L/14.

Dataset		Original				Adversarial Fine-tuning				Test-Time Defense								△					
		CLIP		TeCoA		FARE		R-TPT		LPF		HD		Anti-Adv		TTE		TTC		CSR (Ours)			
Type	Name	Clean	Rob.	Clean	Rob.	Clean	Rob.	Clean	Rob.	Clean	Rob.	Clean	Rob.	Clean	Rob.	Clean	Rob.	Clean	Rob.	Clean	Rob.		
General	ImageNet	69.9	0.6	69.2	67.5	63.9	61.5	71.2	60.0	64.2	43.2	66.4	10.1	68.0	37.1	71.5	32.4	54.7	35.8	68.0	64.1	-1.9	+63.5
	CIFAR10	93.4	1.2	73.7	73.7	76.6	76.5	90.2	82.1	94.3	71.0	92.1	40.5	89.3	78.5	92.3	47.0	94.1	18.4	90.7	83.6	-2.7	+82.4
	CIFAR100	65.0	0.1	44.0	43.8	45.9	45.7	65.7	58.3	72.8	40.3	67.9	26.7	64.7	51.8	72.9	37.9	71.0	7.0	62.9	60.5	-2.1	+60.4
	STL10	99.4	14.1	93.1	93.1	96.2	96.1	98.8	93.4	99.2	91.7	98.6	67.8	99.0	93.3	98.6	88.9	99.4	53.2	99.2	91.2	-0.2	+77.1
	Caltech101	86.2	4.5	80.8	80.8	85.3	85.0	89.0	81.6	86.3	77.5	84.7	45.2	86.0	72.6	91.2	73.5	81.6	41.6	85.3	82.1	-0.9	+77.6
	Caltech256	88.3	3.7	79.2	78.7	83.9	82.8	90.5	85.4	87.4	77.9	86.2	39.5	88.0	74.3	89.9	71.3	82.0	44.0	87.3	83.2	-1.0	+79.5
Fine-G	OxfordPets	93.5	0.3	76.1	72.9	86.6	79.4	94.2	81.4	88.3	61.7	90.5	13.9	91.7	61.1	90.1	36.0	84.8	46.8	93.1	76.4	-0.4	+76.1
	Flowers102	73.5	0.5	35.6	34.0	55.0	50.8	71.5	60.8	72.5	50.1	70.9	10.3	73.5	46.3	73.0	34.9	66.0	33.6	73.3	67.0	-0.2	+66.5
	Food101	90.8	0.1	36.2	34.8	49.4	48.0	90.6	79.3	86.8	61.2	88.7	7.0	87.7	53.1	89.8	36.8	68.3	47.9	90.6	85.8	-0.2	+85.7
	StanfordCars	79.1	0.2	34.5	24.7	64.7	52.3	77.5	59.8	67.6	33.9	68.8	5.8	76.8	31.6	73.4	21.4	61.9	30.3	76.9	65.1	-2.2	+64.9
Scene	SUN397	66.8	0.3	47.8	45.8	57.1	57.7	69.9	61.5	65.6	45.3	64.9	11.5	68.5	38.0	69.4	22.1	56.4	33.0	65.3	65.2	-1.5	+64.9
	Country211	23.7	0.0	5.2	4.7	8.3	7.3	24.2	13.4	22.8	7.1	21.1	0.8	21.9	6.0	26.2	2.3	13.8	6.3	23.0	26.4	-0.7	+26.4
	FGVCAircraft	29.4	0.0	10.6	15.1	21.3	22.2	33.2	20.7	26.1	11.1	26.5	1.4	26.5	10.7	30.2	5.3	23.4	12.1	25.8	32.5	-3.6	+32.5
	EuroSAT	54.8	0.1	19.3	19.2	12.3	12.3	38.8	33.6	53.2	19.0	47.5	11.5	46.9	30.4	41.1	12.0	52.1	7.7	54.7	41.3	-0.1	+41.2
Domain	DTD	53.2	0.7	33.2	32.5	37.3	35.8	53.8	44.4	48.9	35.2	52.3	15.1	50.3	33.5	52.5	26.6	42.4	25.6	50.9	50.4	-2.3	+49.7
	PCAM	49.6	0.2	59.1	58.7	59.7	59.4	43.6	50.4	49.9	48.8	50.4	35.4	50.2	49.1	50.8	50.6	50.1	16.6	51.0	59.2	+1.4	+59.0
All	Avg.	69.8	1.7	49.9	48.8	56.5	54.6	68.9	60.4	67.9	48.0	67.3	21.4	68.1	54.2	69.6	37.4	62.6	28.7	68.6	64.6	-1.2	+62.9

Table 9. Performance comparison across different dataset types and method categories on CLIP-B/32.

Dataset		Original				Adversarial Fine-tuning				Test-Time Defense								△					
		CLIP		TeCoA		FARE		R-TPT		LPF		HD		Anti-Adv		TTE		TTC		CSR (Ours)			
Type	Name	Clean	Rob.	Clean	Rob.	Clean	Rob.	Clean	Rob.	Clean	Rob.	Clean	Rob.	Clean	Rob.	Clean	Rob.	Clean	Rob.	Clean	Rob.		
General	ImageNet	57.8	0.2	51.2	47.6	42.4	40.0	57.4	30.2	52.0	17.4	55.2	3.5	55.7	10.8	61.3	24.1	44.0	24.6	56.8	37.1	-1.0	+36.9
	CIFAR10	86.1	0.6	50.3	50.2	47.2	46.9	76.7	35.1	84.9	27.2	86.5	4.2	84.4	41.8	86.0	33.7	87.6	43.3	86.1	58.1	+0.0	+57.5
	CIFAR100	57.2	0.3	34.8	34.9	28.8	28.6	41.0	14.7	56.0	10.3	61.6	4.2	53.5	20.9	58.8	15.5	58.8	19.1	57.2	29.8	+0.0	+29.5
	STL10	96.2	12.3	80.8	80.4	83.4	83.1	96.5	78.5	96.0	67.2	95.2	32.6	95.3	67.8	97.4	84.8	96.5	72.5	96.2	66.2	+0.0	+53.9
	Caltech101	82.3	6.3	78.2	76.2	80.2	78.7	84.9	29.4	81.0	56.7	81.9	29.1	83.5	50.1	83.2	65.7	82.5	52.1	81.2	59.0	-1.1	+52.7
	Caltech256	80.3	4.1	66.6	64.1	75.6	72.8	80.8	63.5	78.6	49.3	78.8	21.7	79.2	43.1	78.5	60.0	77.3	49.2	79.2	55.0	-1.1	+50.9
Fine-G	OxfordPets	84.2	0.2	68.6	64.3	67.5	61.6	84.2	60.2	74.6	25.2	84.2	6.4	83.6	19.9	81.7	24.8	82.2	30.7	83.9	49.4	-0.3	+49.2
	Flowers102	62.7	0.8	21.5	22.6	44.3	42.7	59.2	35.2	57.8	25.0	59.8	6.2	60.9	14.2	61.5	14.2	61.9	26.4	62.6	32.0	-0.1	+31.2
	Food101	80.4	0.1	24.1	22.1	38.3	36.6	82.1	57.1	71.0	20.3	79.7	3.6	78.5	11.4	79.9	46.0	72.7	36.5	79.4	57.7	-1.0	+57.6
	StanfordCars	59.9	0.0	26.1	20.5	60.3	52.1	60.2	28.1	44.4	5.1	50.5	3.2	58.1	4.9	51.2	26.6	49.0	16.3	59.6	25.4	-0.3	+25.4
Scene	SUN397	61.9	0.8	32.2	32.9	42.2	40.1	63.1	54.2	59.3	21.3	58.1	6.1	61.7	13.2	62.2	18.0	53.1	31.2	61.1	48.3	-0.8	+47.5
	Country211	15.7	0.0	2.2	2.7	4.1	4.4	14.3	5.0	13.1	1.2	12.1	0.0	12.9	0.8	16.3	1.2	12.6	3.7	15.5	12.1	-0.2	+12.1
	FGVCAircraft	17.3	0.0	4.3	7.3	10.1	12.2	19.7	13.6	16.7	2.0	15.7	1.1	14.3	2.0	19.8	5.1	11.4	9.2	17.2	16.7	-0.1	+16.7
	EuroSAT	34.2	0.0	14.4	14.4	17.4	17.4	27.7	21.4	29.5	1.5	35.3	2.1	28.7	13.7	28.8	10.2	33.6	13.9	34.2	26.1	+0.0	+26.1
Domain	DTD	43.3	1.7	25.8	24.9	32.3	31.6	39.6	32.6	39.9	18.0	40.3	11.4	40.9	15.6	44.2	23.2	42.9	22.1	42.4	25.8	-0.9	+24.1
	PCAM	48.9	24.8	55.7	55.6	51.0	50.8	55.4	41.2	48.7	48.2	49.0	39.8	48.8	48.3	54.5	38.7	48.8	44.2	49.1	50.3	+0.2	+25.5
All	Avg.	60.5	3.3	39.8	38.8	45.3	43.7	57.9	37.6	56.5	24.7	59.0	11.0	58.8	23.7	57.2	30.7	57.2	30.9	60.1	40.6	-0.4	+37.3

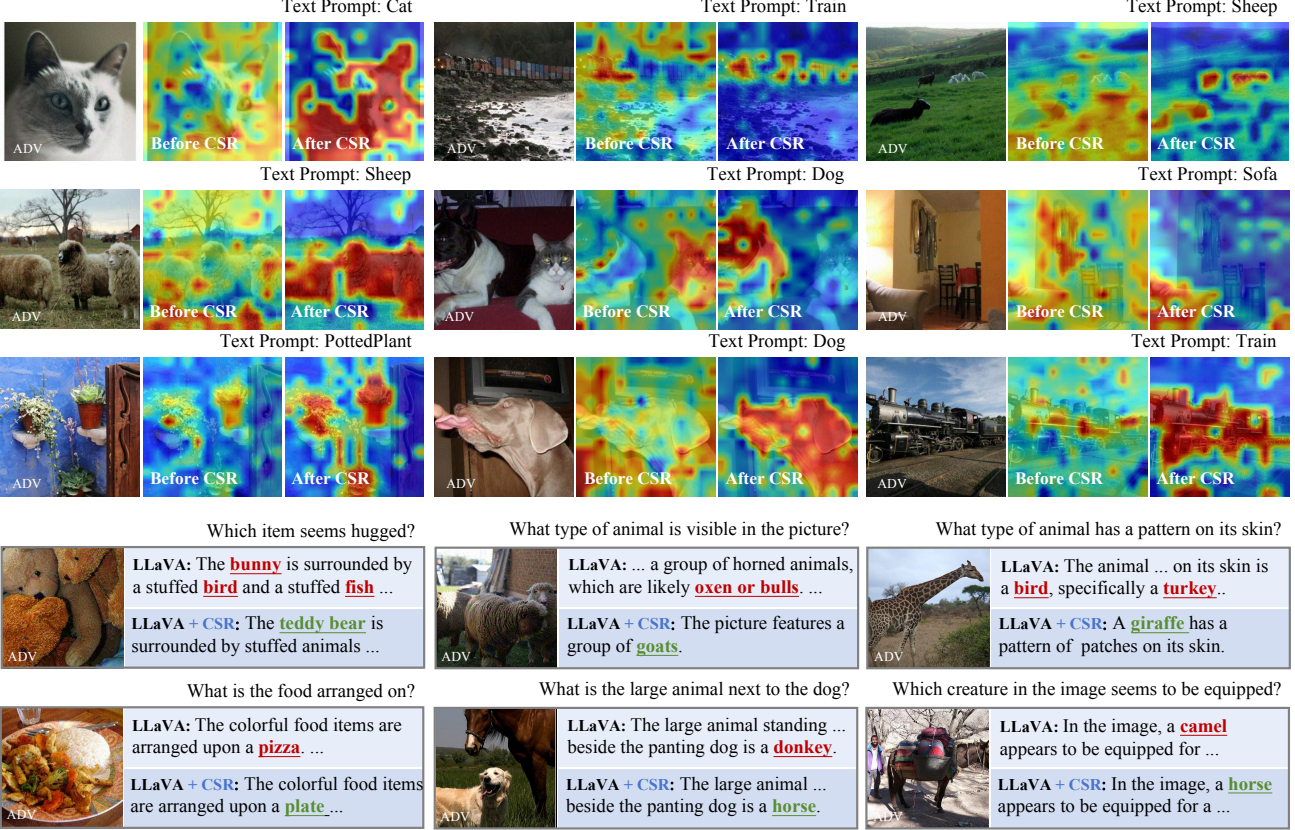


Figure 7. Additional Visualizations.

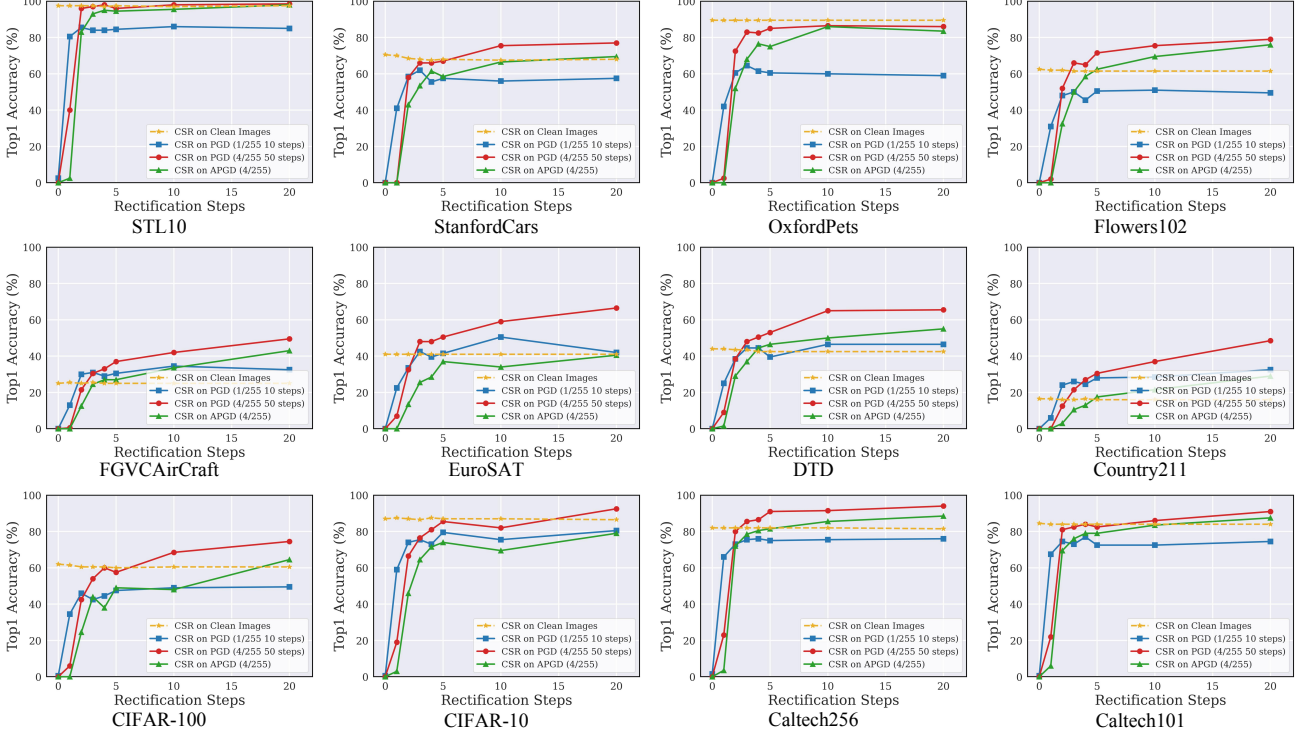


Figure 8. Ablation on the Rectification Steps.

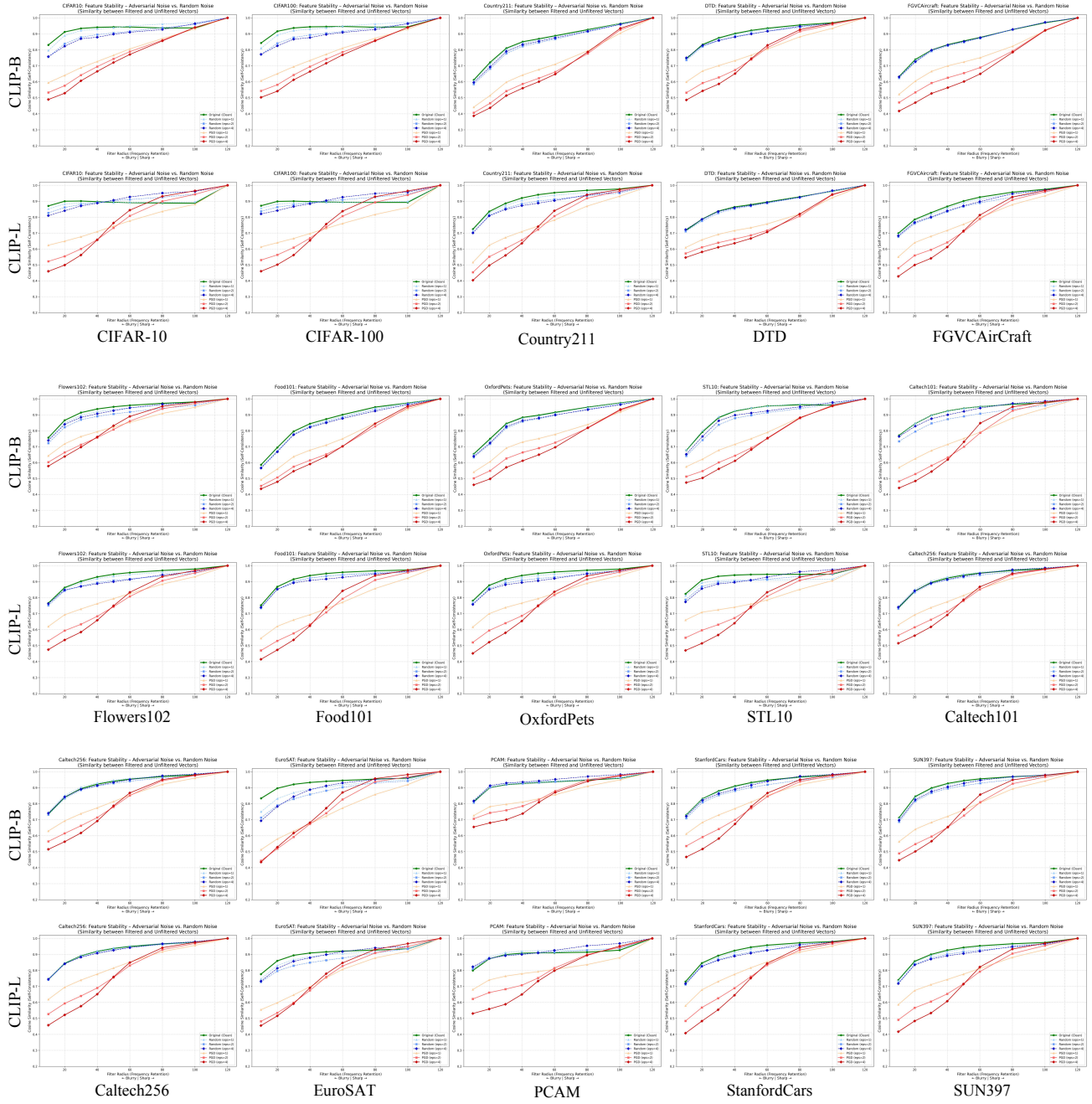


Figure 9. Spectral Analysis of CLIP Feature Consistency on widely used 15 Benchmark Datasets.

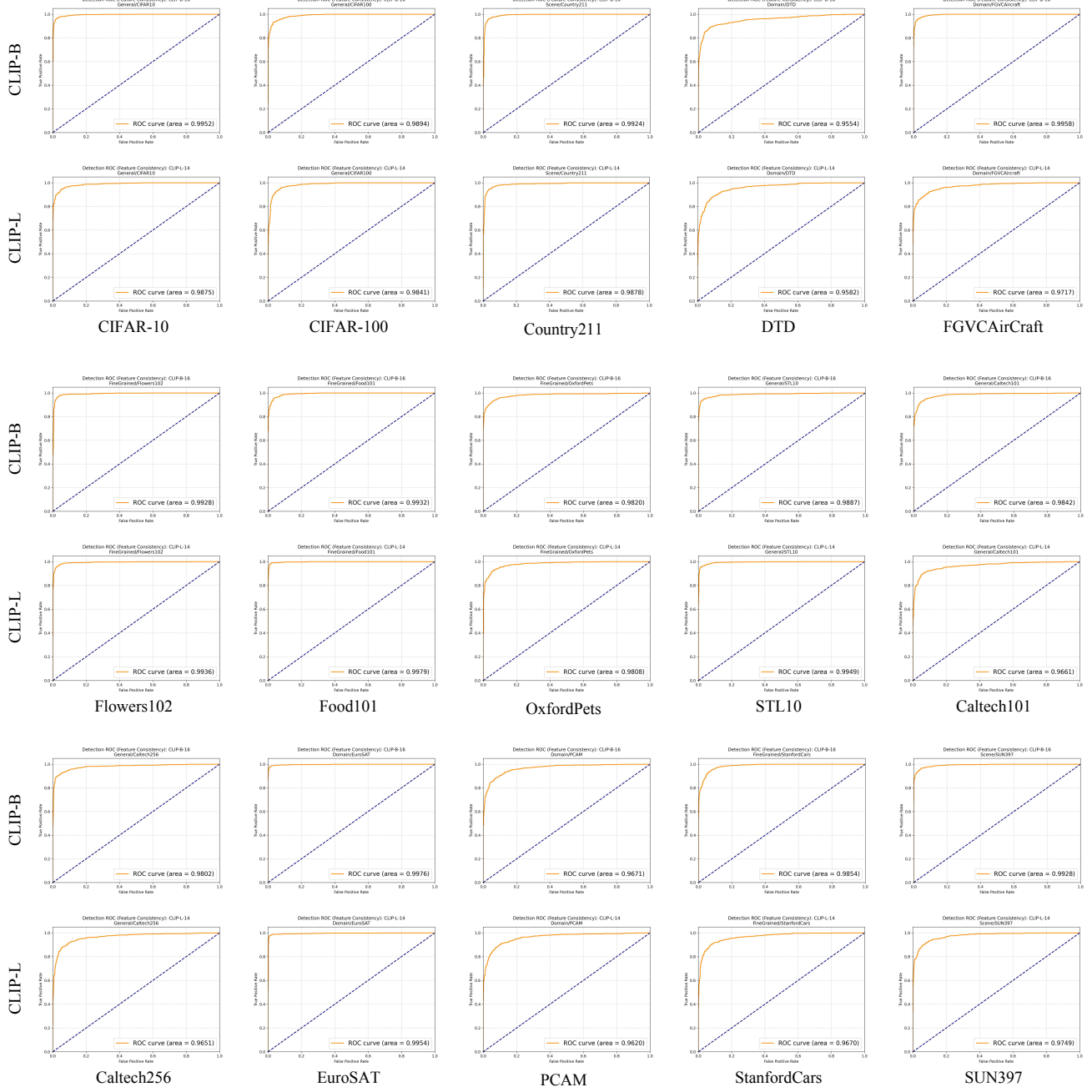


Figure 10. AUC curves for adversarial sample detection on 15 benchmark datasets.